Standard Title Page - Report on Federally Funded Project

1. Report No. FHWA/VTRC 06-CR5	2. Government Accession No.	3. Recipient's Catalog No.
4. Title and Subtitle Construction of a Virginia Short-Span Bridge with the Strongwell 36-Inch Double-Web I-Beam		5. Report Date October 2005
		6. Performing Organization Code
7. Author(s) Thomas E. Cousins and John J. Lesko		8. Performing Organization Report No. VTRC 06-CR5
9. Performing Organization and Address Virginia Transportation Research Council 530 Edgemont Road Charlottesville, VA 22903		10. Work Unit No. (TRAIS)
		11. Contract or Grant No. 55941
12. Sponsoring Agencies' Name and Address Virginia Department of Transportation FHWA 1401 E. Broad Street P.O. Box 10249 Richmond, VA 23219 Richmond, VA 23240		13. Type of Report and Period Covered Final
		14. Sponsoring Agency Code
15. Supplementary Notes		

16. Abstract

The Route 601 Bridge in Sugar Grove, VA, spans 39 ft over Dickey Creek. The bridge is the first to use the Strongwell 36-in-deep fiber-reinforced polymer (FRP) double-web beam (DWB) in a vehicular bridge superstructure. Construction of the new bridge was completed in October 2001, and field testing was undertaken shortly thereafter as well as in June of 2002 to assess any potential changes in structural performance.

This paper details the field evaluation of the Route 601 Bridge. Using midspan deflection and strain data from the October 2001 and June 2002 field tests, AASHTO bridge design parameters were determined, namely wheel load distribution factor g, dynamic load allowance IM, and maximum deflection. The wheel load distribution factor was determined to be S/4, a dynamic load allowance was determined to be 0.50, and the maximum deflection of the bridge was L/1110. Deflection results were lower than the AASHTO L/800 limit. This discrepancy is attributed to partial composite action of the deck-to-girder connections, bearing restraint at the supports, and contribution of guardrail stiffness. It was found that diaphragm removal had a small effect on the wheel load distribution factor.

An examination of the 36-in DWB capacity and failure mode indicates that the strength of the girder is controlled by compression failure in the flange and not shear failure, as originally thought. An attempt to predict the girder fatigue performance shows that small losses in bending stiffness would be expected at fatigue loads 26% of the ultimate capacity, which was confirmed through experiments. Moreover, there is no concern that fatigue alone will cause a failure during the reasonable life of the structure as presently operated.

17 Key Words Composite materials, fiber reinforced polymer, bridges, girders, timber deck, AASHTO bridge design	18. Distribution Statement No restrictions. This document is available to the public through NTIS, Springfield, VA 22161.		
19. Security Classif. (of this report) Unclassified	20. Security Classif. (of this page) Unclassified	21. No. of Pages 42	22. Price

Form DOT F 1700.7 (8-72)   Reproduction of completed page authorized

FINAL CONTRACT REPORT

CONSTRUCTION OF A VIRGINIA SHORT-SPAN BRIDGE
WITH THE STRONGWELL 36-INCH DOUBLE-WEB I-BEAM

Thomas E. Cousins
Associate Professor
Via Department of Civil and Environmental Engineering
Virginia Polytechnic Institute & State University

John J. Lesko
Associate Professor
Department of Engineering Science and Mechanics
Virginia Polytechnic Institute & State University

ABSTRACT

The Route 601 Bridge in Sugar Grove, VA, spans 39 ft over Dickey Creek. The bridge is the first to use the Strongwell 36-in-deep fiber-reinforced polymer (FRP) double-web beam (DWB) in a vehicular bridge superstructure. Construction of the new bridge was completed in October 2001, and field testing was undertaken shortly thereafter as well as in June of 2002 to assess any potential changes in structural performance.

This paper details the field evaluation of the Route 601 Bridge. Using midspan deflection and strain data from the October 2001 and June 2002 field tests, AASHTO bridge design parameters were determined, namely wheel load distribution factor g, dynamic load allowance IM, and maximum deflection. The wheel load distribution factor was determined to be S/4, a dynamic load allowance was determined to be 0.50, and the maximum deflection of the bridge was L/1110. Deflection results were lower than the AASHTO L/800 limit. This discrepancy is attributed to partial composite action of the deck-to-girder connections, bearing restraint at the supports, and contribution of guardrail stiffness. It was found that diaphragm removal had a small effect on the wheel load distribution factor.

An examination of the 36-in DWB capacity and failure mode indicates that the strength of the girder is controlled by compression failure in the flange and not shear failure, as originally thought. An attempt to predict the girder fatigue performance shows that small losses in bending stiffness would be expected at fatigue loads 26% of the ultimate capacity, which was confirmed through experiments. Moreover, there is no concern that fatigue alone will cause a failure during the reasonable life of the structure as presently operated.

FINAL CONTRACT REPORT

CONSTRUCTION OF A VIRGINIA SHORT-SPAN BRIDGE
WITH THE STRONGWELL 36-INCH DOUBLE-WEB I-BEAM

Thomas E. Cousins
Associate Professor
Via Department of Civil and Environmental Engineering
Virginia Polytechnic Institute & State University

John J. Lesko
Associate Professor
Department of Engineering Science and Mechanics
Virginia Polytechnic Institute & State University

INTRODUCTION

According to a report to the United States Congress published by the U.S. Department of Transportation, 167,993 of 587,755 of the nation's bridges have been labeled as "deficient", roughly 29% of the total. Structurally deficient bridges are about half of the "deficient" bridges in the US and are characterized by a low load rating, deterioration in its substructure or deterioration in its superstructure. The cost for improvements on these deficient bridges as well as the backlog of bridge needs was estimated at $87.3 billion (AASHTO 2001). Maintaining the current backlog of deficiencies would require an annual investment of 5.8 billion dollars per year, while offsetting the total backlog over the next twenty years will require a 10.6 billion dollar annual investment (AASHTO 2001). The expense of maintaining our highway and local bridges has motivated engineers to seek design alternatives. Fiber Reinforced Polymer (FRP) materials offer a potentially cost effective solution for rehabilitating and extending the life of our nation's bridge infrastructure.

FRP materials possess a high strength to weight and stiffness to weight ratio compared to traditional bridge superstructure components made of steel or concrete. As a result of the high specific properties handling and installation costs are reduced compared to a structurally equivalent design in traditional materials. The reduced weight of FRP elements allows for rapid construction and placement decreasing the length of traffic delays due to road closings, which can have a considerable impact on local economies affected by detours. More importantly FRP structural equivalent elements decrease dead loads subsequently increasing live load ratings.

FRP materials also exhibit corrosion resistant properties. The use of deicing salts for harsh climates accelerates corrosion in steel and reinforced concrete structures. However, FRP is not susceptible to corrosion under normal traffic conditions, which could increase the durability of a bridge and decrease the frequency of bridge rehabilitation and replacement. FRP's

durability can also create lower life cycle costs, which include the cost for maintenance, repair, inspection, disposal, and replacement of a structure (Nystrom et al. 2001).

The pultruded FRP market in infrastructure has been developing since the early 1990s. The pultrusion manufacturing process involves the pulling of reinforcing fibers and resin matrix materials through a series of forming dies that shape and cure the material (Hyer 1998). It is estimated that the FRP market in infrastructure will continue to grow at a rate of 25% each year, especially in bridge decks and bridge superstructures for both pedestrian and vehicular bridge applications that utilize pultruded structural shapes (Kliger & Loud, 2001). Awareness of the advantages of FRP is increasing among engineers. However, because the use of FRP materials in bridges has only spanned a little more than a decade, its acceptance into the bridge industry is still evolving and remains a work in progress.

Pultruded FRP materials present several disadvantages when used in bridge engineering applications. Material costs are high relative to traditional construction materials. Further studies and emphasis on life cycle costs may further advance the routine use of pultruded FRP shapes. Other impediments to the use of FRP structures include an absence of design specifications and a lack of experience in working with the material.

Design engineers are familiar with using traditional materials, such as steel and concrete, for bridge construction as well as using standard procedures presented in established design codes. The lack of a FRP design code has caused civil engineers to not consider FRP as alternate design methods are required. These design procedures are not standardized and are not available for routine implementation.

PURPOSE AND SCOPE

This paper reports the findings of a research project concerned with the rehabilitation of the Rt. 601 bridge over Dickey Creek utilizing the pultruded double web beam manufactured by Strongwell, Corp. (Strongwell, 2000). The Virginia Department of Transportation (VDOT) commonly uses steel wide flange rolled shapes with a timber deck and asphalt wearing surface for short span, rural stream crossings. For the Dickey Creek Bridge the steel girders normally used in this type of bridge were replaced with the pultruded double web beam. The Rt. 601 bridge replacement project serves several purposes. One purpose was to replace an existing simple span bridge that was exhibiting severe corrosion and classified as a structurally deficient bridge. The deteriorated bridge, near rural Sugar Grove, VA, experiences a low traffic volume of mostly small to medium sized vehicles. Thus the bridge also served as a demonstration of the use of pultruded FRP girders in a short span bridge. Moreover, the Rt. 601 bridge serves as an opportunity to study the structural behavior of a FRP superstructure and assess the applicability of AASHTO design procedures developed for traditional construction materials.

A preliminary design of the bridge utilizing a timber deck and FRP girders followed laboratory testing of the individual girders (Waldron 2001, Hayes 2001). Construction of the bridge began in June of 2001 and was completed in October 2001. The four month construction time was primarily due to the construction time required for the cast-in-place reinforced concrete

abutments and back walls which were delayed due to two high water events. The FRP double web beams were set in four hours with a small capacity crane. Following construction of the bridge, the first of two controlled vehicle field tests was performed to assess in-service performance and to provide general understanding of bridge behavior using pultruded FRP girders. Second and third field tests were performed in June of 2002 and October of 2003 in an effort to assess if any changes occurred as well as to examine the influence of diaphragms (Restrepo 2002, Kassner 2004). Additional work was undertaken to assess fatigue performance of the girders. Both analytical and experimental work focused on understanding the failure modes and the mechanisms that controlled life in an effort to ensure safe operation given the expected loading (Hayes 20030.

BACKGROUND

Tom's Creek Bridge: Previous Experience

The Tom's Creek Bridge in Blacksburg, VA, is a similar replacement project completed in June of 1997. The town of Blacksburg, the Virginia Transportation Research Council (VTRC), the Virginia Department of Transportation (VDOT) and Virginia Tech cooperated to construct a new bridge using the pultruded 8 in deep FRP composite double web beams (DWB) manufactured by Strongwell (Hayes, 1998, Hayes, 2000).

The Tom's Creek Bridge supports two lanes of traffic with a clear span of 18 ft and a roadway width of 22 ft.   The 24 Strongwell 8-in DWBs support a glue laminated timber panel deck with an asphalt wearing surface. The average bending modulus of each of the Strongwell 8 in beams was experimentally determined to be 6670 ksi in bending mode (Hayes 1998).

After construction of the Tom's Creek Bridge, five live load tests were performed on six-month intervals starting in the fall of 1997 (Neely, 2000). Deflections and strains were measured, but tests were also performed in order to determine the wheel load distribution factor and the dynamic load allowance (DLA). The bridge was load tested with a single tandem axle dump truck filled with gravel with an average weight of 48.8 kips. A wheel load distribution factor of 0.10 was experimentally determined, or 10 % of a truck wheel load which translates into an equivalent AASHTO distribution factor per wheel line of S/4.6. Based on the results from the Tom's Creek Bridge load tests, it was proposed that AASHTO design requirements for a glue-laminated deck on steel stringer bridge be adopted for the glue-laminated deck on FRP composite girder Tom's Creek Bridge. The maximum deflection of 0.43 in resulted in a corresponding deflection of L/488, which satisfied the L/500 limit for the AASHTO standard specification criterion for an all timber bridge. However, this deflection value exceeded the L/800 criterion for a timber deck on steel girder bridge (Neely, 2000).

From the live load tests that were performed on the bridge, a maximum dynamic load allowance (DLA) of 0.90 was determined, suggesting the dynamic load effect of a dump truck traveling at a speed of 40 mph is almost twice as much as when its load is placed in a static condition. The result was significantly greater than the 30% AAHSTO Standard Specification DLA value assumed in the design (AASHTO, 1996) and further evaluation of the dynamic behavior of bridges like the Tom's Creek Bridge was recommended. Significant reflective cracking of the asphalt wearing surface was observed after two years of service.

Route 601 Bridge: History and Rehabilitation

The original Route 601 Bridge was constructed in 1932 in rural Sugar Grove, VA. Its steel superstructure spanned 30 ft. The new structure was completed in October, 2001 as a result of collaborative effort between VDOT, VTRC, Strongwell, Virginia Tech, and the Federal Highway Administration (FHWA). The main load carrying members of the bridge are the Strongwell 36 in hybrid DWB (as shown in Figure 1), which is very similar to the 8 in deep DWB used in the Tom's Creek Bridge. The top and bottom flanges contain both E-glass and carbon fibers in a vinyl ester resin, while the web material and sub-flanges are composed of E-glass fibers in a vinyl ester resin.

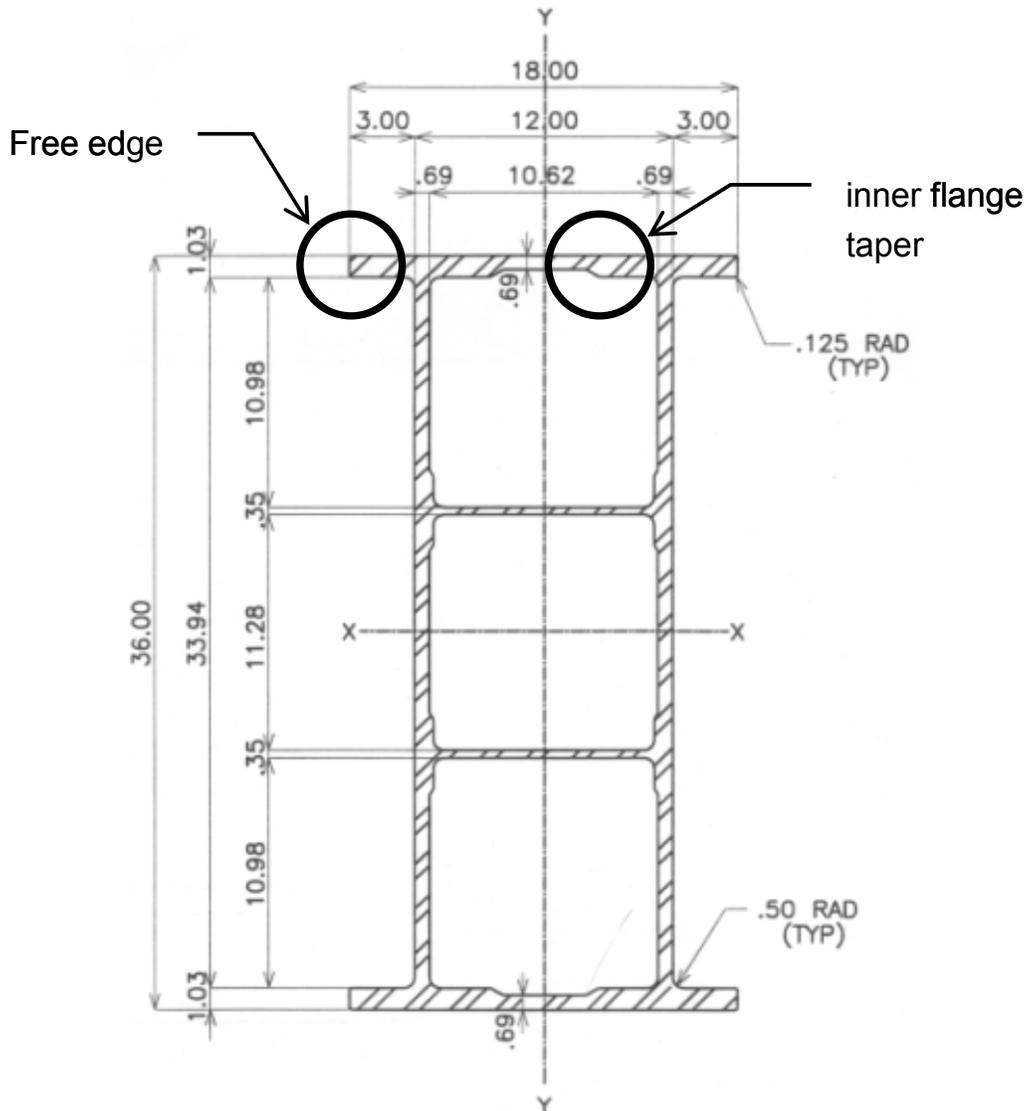**Figure 1. Strongwell 36-in Double-Web Beam. All dimensions in inches.**

A preliminary design was performed for the Rt. 601 Bridge to determine the girder layout and spacing (Waldron 2001, Hayes 2001). The bridge was designed for an AASHTO HS20-44 loading. A deflection target of L/800 was used along with an assumed dynamic load allowance of 30%, a clear span of 38 ft, and a curb-to-curb roadway width of 28 ft. Based on previous

research from the Tom's Creek Bridge project, conservative mechanical properties were assumed in the preliminary design: Young's Modulus (E) of 6,000 ksi and a shear stiffness (KGA) of 20 Msi-in^2 were used. Table 1 gives actual, tested values of E and KGA for the beams used in the Route 601 Bridge. The girder distribution factor from the AASHTO Standard Specification (AASHTO, 1996) for a glue-laminated timber deck on steel girder superstructure was selected. By using the L/800 target, a 3.5 ft transverse girder spacing was selected. With a 28 ft wide roadway and a spacing of 3.5 ft, 8 girders were selected for the bridge cross section. A deflection based design approach was used, and it was found that the maximum load effect from placing the HS20-44 truck load on the bridge with the assumed distribution and dynamic load allowance resulted in a deflection that was comparable to the initial L/800 criteria.

Table 1. Summary of Properties of Individual 91.4 cm (36 in) DWB

| Beam #	E (ksi)	KGA (ksi-in^2)
1	6,450	24,250
2	6,350	23,050
3	6,050	24,780
4	6,060	24,780
5	5,880	30,730
6	6,180	26,170
7	6,200	34,120
8	6,590	25,190

METHODS

Pre-Construction Testing

Before construction of the bridge could begin VDOT required the following testing to be conducted:

1. Test each of the eight girders to be used in the bridge to five times the design service load (197 ft-kips). This was considered a proof test to insure manufacturing quality and behavior without damage to this load level.

2. Test one 36 in double web beam to failure. The purpose of this test was to determine the failure moment and failure load to insure a proper safety factor against failure exists and to define the failure mode to aid in future inspections of the bridge.

3. Test another 36 in double web beam with attached timber deck with the girder to deck connection detail in place. The girder to deck connection was designed to give partial composite action between the deck and girder. Even though the bridge was designed assuming no composite action exists, it was necessary to determine if any partial composite action was provided for future applications.

The eight 36 in DWB supported ten creosote treated, glue-laminated timber deck panels, each 4 ft x 30 ft x 5 1/8 in thick. The total transverse width of the bridge was 31 ft 9 in, with a 28 ft roadway width between the glue-laminated timber guardrails (Figure 2). An asphalt wearing surface was placed over the timber deck. The 36 in DWB spanned 39 ft between centers of supports. The beams rested on 9 in x 14 x 2 in neoprene bearing pads. Concrete abutments that replaced the existing rubble abutments supported the steel reinforced neoprene bearing pads (Waldron 2001). Three diaphragms were placed in between each of the girders, two at the ends and one intermediate diaphragm located 1 ft east of mid-span. The deck to girder connection involved steel double angles bolted to the webs of the double web beams and to the underside of the timber deck panels. A photograph of this connection is shown in Figure 3. Note that this connection was not intended to induce composite action.
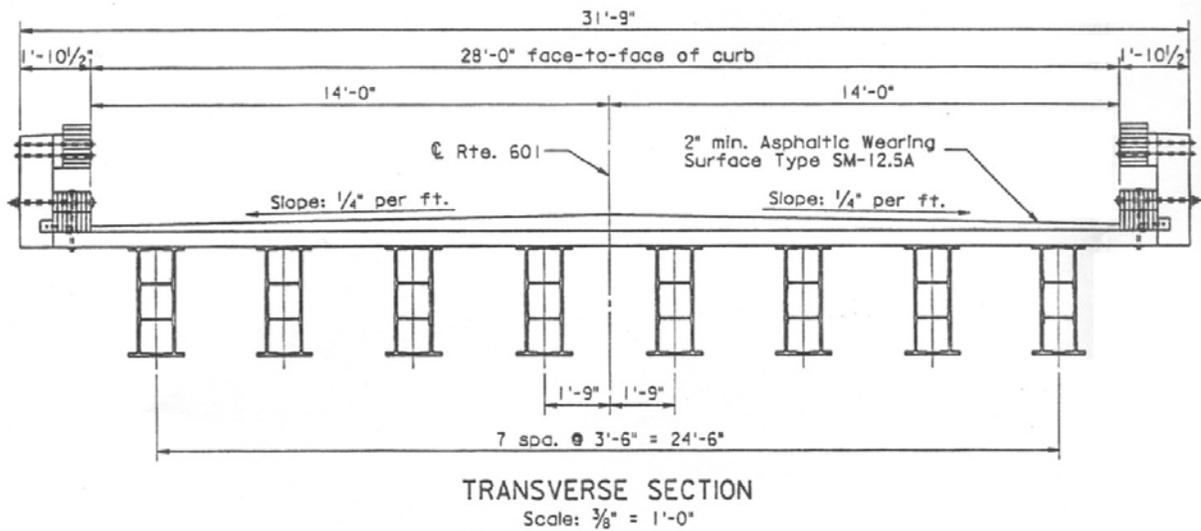
Figure 2. Rt. 601 Bridge Cross Section.

Figure 3. Photograph of Deck to Girder Connection.

Route 601 Bridge Live Load Tests

The Rt. 601 Bridge was instrumented with strain gages and deflectometers in order to evaluate its behavior during controlled vehicle load testing. The same instrumentation was used for the October 2001 and the June 2002 live load test.

The strain gages used were a quarter of an inch in length and had nominal resistance of 350 ohms. All of the gages were applied at mid-span on the bottom of the bottom flange of the eight girders and strain was measured in the direction of traffic, which is along the longitudinal axis of the beam. During the fall and summer field tests, some of the strain gages exhibited excessive noise up to ± 30 $\mu\varepsilon$. A ten point floating average was taken to reduce the noise to a level approximately within ± 5 $\mu\varepsilon$. The deflectometers were calibrated at different deflections levels to within 0.0003 in accuracy before each live load test.

A high speed data acquisition system with test control software was used for the field data collection. A scanning rate of 400 samples per second per channel was used to permit adequate data collection for controlled vehicle load tests.

Two three-axle VDOT dump trucks filled with gravel from a local quarry were used for the field test of the Rt. 601 Bridge. The front and rear axles of each of the trucks were weighed and recorded for the three field tests (October 2001, June 2002, and October 2003) and were approximately equal to the legal load limit for the Rt. 601 bridge. The legal load limit for a three axle truck is approximately 25 tons with the limit on the tandem rear axle as 17 tons. The axle weights and dimensions of the trucks are summarized in Table 2. Note that the same two trucks were used for each live load test and only the weights varied slightly.

Table 2. Test Truck Weights and Dimensions

Live Load Test	Truck #	Total Weight (kips)	Front Axle (kips)	Tandem Axle (kips)	Front to Rear Axle Length (feet)	Transverse Wheel Spacing (feet)
October 2001	1	55.2	17.3	37.6	19.75	6.83
	2	55.2	14.9	40.3	18.5	6.67
June 2002	1	55.4	14.2	41.2	19.75	6.83
	2	55.9	16.4	39.4	18.5	6.67
October 2003	1	55.2	16.6	38.6	19.75	6.83
	2	55.2	15.2	40.0	18.5	6.67

Test truck axle positions were selected to introduce maximum response in the supporting girders. The loading configurations used are shown in Figure 4 and are further defined as follows:
   a) One wheel line centered over the first interior girder (Girder 7)
   b) One wheel line centered over the first interior girder (Girder 2)
   c) Truck centered in middle of bridge
   d) Side-by-side trucks with one wheel line centered over each exterior girder
   e) One wheel line centered over the exterior girder (Girder 8)
   f) One wheel line centered over the exterior girder (Girder 1)

a)

b)

c)

d)

e)

f)
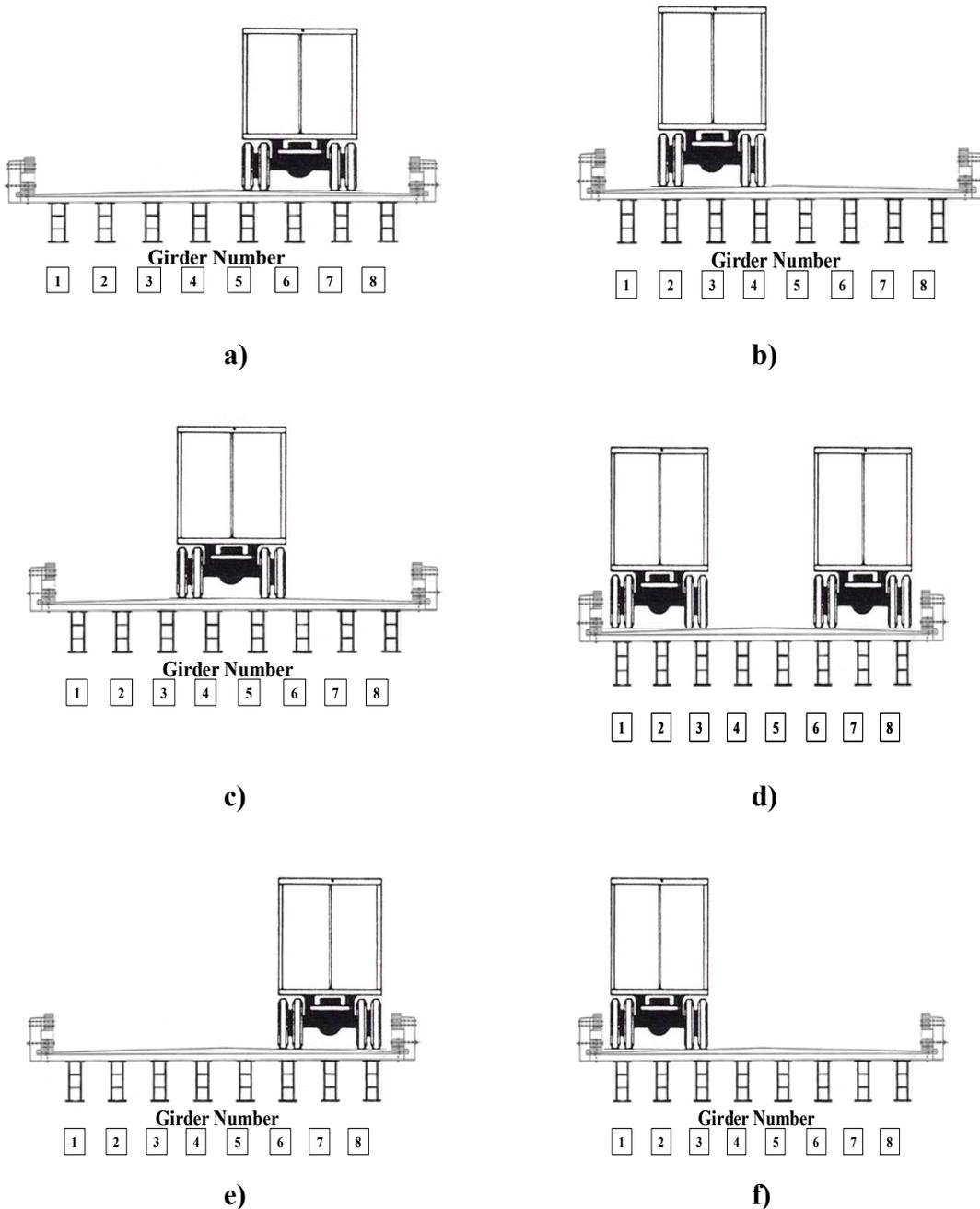
Figure 4. Truck Crossing Axle Orientations.

In addition to "static" loadings various speeds were used to simulate different dynamic loading conditions. In the Fall 2001 field test, three different speeds were used. The truck crossed at a creep speed of approximately 2 mph to simulate a static loading condition of the bridge. An intermediate speed of 25 mph followed to simulate a pseudo-dynamic condition of the bridge. The final speed attempted was determined by the fastest speed the truck could travel safely across the bridge, approximately 40 mph. The dynamic tests of 25 mph and 40 mph were only performed for truck axle positions a), b) and c). Dynamic tests were not performed for axle positions d), e), and f) due to safety concerns. The roadway approaches to the bridge lacked guardrails and the approaches were narrower than the bridge width.

An additional speed of 15 mph was used for the June 2002 field test. Results from the initial field test indicated that ramping effects due to settling at the approaches caused the truck to produce lower strains with increasing speed. An additional speed between the static and 40 km/h case was used to further investigate this condition.

The June 2002 field test included additional truck runs to investigate the behavior of the bridge resisting load without the use of diaphragms. At the conclusion of the static and dynamic runs of the aforementioned truck passes, the intermediate diaphragms between girders 5 and 8 were removed. Field testing sequence proceeded with two additional positions, truck axle orientations a) and e). The additional two truck tests were performed only at static speeds. In all cases a total of five repetitions of each truck position at each speed were recorded.

36-inch DWB Strength and Fatigue Performance

Characterization of Capacity & Failure Mode

The first objective of this effort was to predict the static strength of the 36 inch DWB. The first step is to identify the failure mode, based on the experience with the 8 inch section, failure of the 36 inch DWB is hypothesized to occur by delamination at either the free edge or the inner flange taper (see Figure 1). The possibility of compression failure of the carbon fiber plies was also investigated. Post-failure inspection of the beams coupled with a detailed global and local finite element analysis (ANSYS) was undertaken to identify the failure mode and location (Hayes 2003).

Approach to the Prediction of Fatigue Performance

Having determined the failure mode and developed means to predict the strength, the second objective of this study is to predict the fatigue life of the DWB as tested under transverse loading. The stress analysis is incorporated into a life prediction code using the critical element approach (Reifsnider and Case 2002). Stiffness reduction in off-axis plies was modeled using empirical data from coupon studies. The remaining strength of the carbon plies will be tracked using fatigue-life curves obtained from coupon testing. The remaining strengths of the delamination sites may also be monitored. A fatigue-life curve was then constructed for the DWB under transverse loading and compared to experimental data for full-scale fatigue tests. A complete description of the strength and fatigue analysis is detailed by Hayes (2004).

Girder Fatigue Testing

Due to the limited availability of the beams for destructive testing, only two DWBs were tested in fatigue using MTS actuators and control system. The first beam was tested in four-point geometry with loads applied at the third points, as in the static testing. The beam length was slightly over 40 ft, and the center-of-bearing (COB) to COB span length was 39 ft. The beam was loaded to a maximum deflection equal to 0.6 inches, approximately two times the maximum predicted service deflection in the Route 601 Bridge. The corresponding load was 30 kips per actuator, which corresponds to about 30% of the ultimate static failure load (94.5 kips).

A load ratio of R = 0.1 and a frequency of 1.1 Hz was used. The test was stopped after 4.9 million cycles due to mechanical problems.

The second beam was loaded to approximately 60% ultimate failure stress to promote failure within a reasonable time.   This stress level corresponds to 60 kips in the four-point test geometry; however, the capacity of the actuators was only 50 kips. Therefore, the test geometry was changed to a three-point loading geometry to utilize a larger 200 kip actuator that was available. Again, a 39 ft COB-to-COB span length was used; the second beam was slightly longer at 44 ft, yielding a 13 inch overhang on each end. Because three-point test results were not available, the ultimate failure for this geometry was estimated using the static strength prediction2. The predicted strength for the compression failure mode is 68 kip shear capacity or 1835 kip-ft moment capacity. The resulting center point test load was 60% x 2 x 68 kip = 81.6 kip.

In both tests, stiffness reduction was monitored by periodically interrupting the fatigue cycling to perform quasi-static loading tests. During the quasi-static tests, the mid-span deflections and inner corner pad deflections at one end were measured. Furthermore, axial flange strains and web shear strains were measured. The effective bending modulus was calculated using the flange strains, since the deflection measurements are less accurate due to support and load frame deflections. This yields the change in the actual bending stiffness only, which is slightly different than the change in effective bending stiffness calculated using the FEA results. However, the web panels are not expected to experience significant stiffness reduction and the shear deformation accounts for only 15% of the total deflection at the 39 ft span, so the error between the two methods is likely to be small.

RESULTS AND DISCUSSION

Determination of the experimental load distribution factors, dynamic load allowances, and deflections are discussed below. The results are compared with the pre-construction design assumptions as well as design values found in the AASHTO Specifications.

Pre-Construction Testing

Experimental stiffness testing of the Strongwell 36 in DWB was conducted at the Virginia Tech Structures Laboratory. A four point bending test setup with a span of 39 ft was used for each girder. Each beam used in the bridge was proof tested to five times the design service load. Determined properties of each of the eight beams are shown in Table 1.

One 36 in double web beam was tested to failure. This girder experienced linear behavior to failure with a failure moment of about 1400 ft-kips. The failure mode was due to top flange delamination near a load point. The interface between the carbon and glass fiber mats in the top flange is an area high interlaminar stress due to the mismatch of material moduli and hence probably the location and source of failure. Even after failure the beam retained 73% of its pre-test stiffness.

For the testing of the girder to flange connection very little composite action was developed (2 to 4 % depending on the spacing of connections) so it was recommended that enough connections be included in the bridge to resist uplift and braking forces.

Wheel Load Distribution

Girder Distribution Factors (GDFs) were calculated for the Rt. 601 Bridge using both deflection and strain data from the live load truck crossings of the October 2001, June 2002 and October 2003 field tests. Stallings and Yoo (1993) presented previous research on girder distribution factors based on field tests of steel girder bridges and derived the calculation for a particular *i*th girder for strain data when all girders of the same section modulus are used in a bridge:

$$GDF_i = \frac{\varepsilon_i}{\sum_{j=1}^{k} \varepsilon_j} \qquad \text{(Eq. 1)}$$

For the Tom's Creek Bridge field test, Eq. 2 was used to determine GDFs which is a similar approach to that of Stallings and Yoo:

$$GDF_i = \frac{R_i}{\sum_{j=1}^{k} R_j} \qquad \text{(Eq. 2)}$$

where R is the response of a girder, either in strain or deflection. Neely (2001) proceeded to determine distribution factors from both strain and deflection data.

For this research, identical material properties were assumed in the calculation of girder distribution even though young's modulus and the shear stiffness varied among the eight girders due to variability introduced by manufacturing. This variation was judged to be similar to that encountered in a reinforced concrete multi-girder bridge with the same girder cross-sectional dimensions due to the variation in material properties and was therefore not included. In order to convert the load fractions from the above equation to a distribution factor with the same nomenclature to that in the AASHTO *Standard Specification* (AASHTO 1996), the load fractions were divided by the number of wheel lines used. For instance, for a typical single lane truck pass, the load fraction was divided by two, and for multiple (two) lane passes the load fractions were divided by four. GDF results will be reported here per truck wheel line and the values will be presented as a function of the bridge girder transverse spacing.

In order to determine the girder distribution factor for a specific truck crossing, the maximum response for any girder was first determined (**R_i** in Eq.2), and then the time of the maximum response was noted. After establishing the time of maximum response, the summation of each individual girder response at that time was recorded (**$\sum R_j$** in Eq. 2). Figure 5 shows a sample plot from a creep truck crossing of the Rt. 601 bridge with the maximum girder response and associated time labeled. Girder distribution factors were then calculated for each girder per truck crossing using Eq. 2 for both strain and deflection. This procedure was applied to the results from each truck crossing and these results were averaged for each test at each speed.

Center Lane Static Run 1
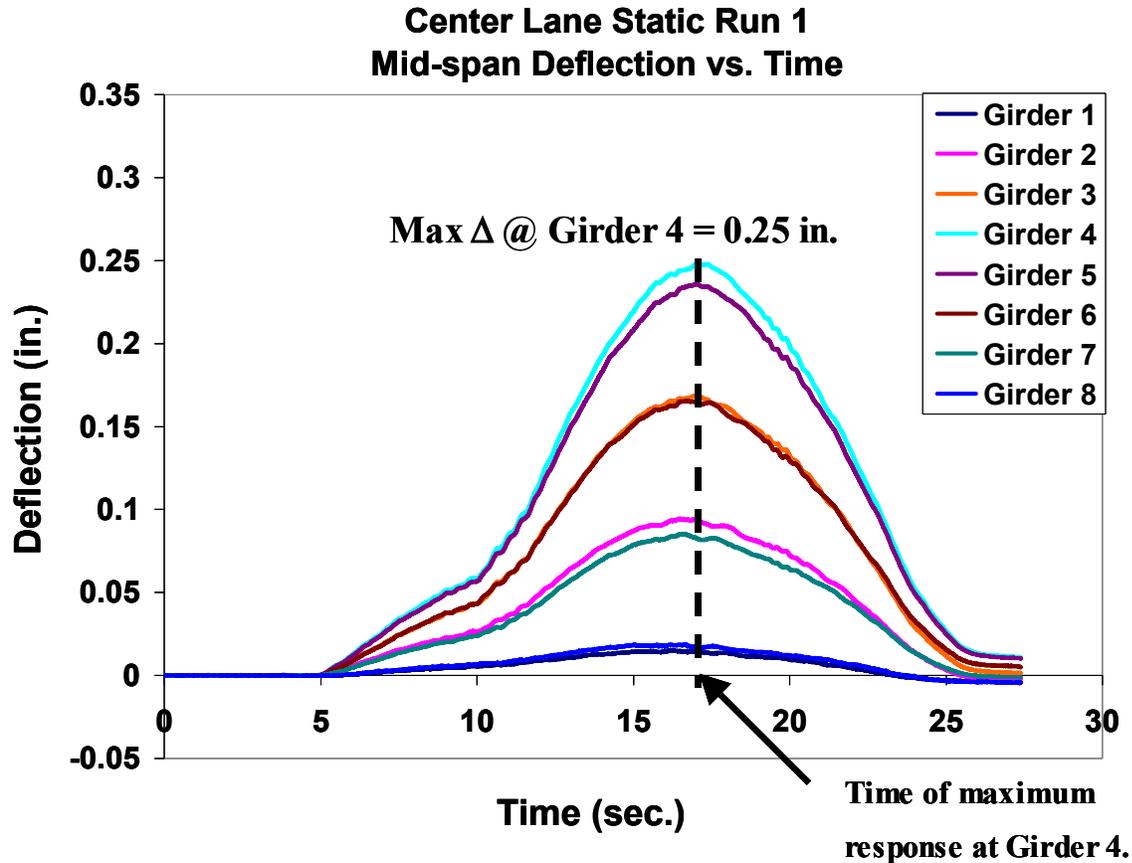**Mid-span Deflection vs. Time**

Figure 5. Example Deflection vs. Time plot. GDF calculations are based on girder responses at time of maximum bridge response.

Wheel load distribution factors are summarized for each test configuration and speed for the fall 2001 and summer 2002 field tests in Table 3. Generally, the distribution factors from the three tests were approximately equal and the distribution factors determined from strain and deflection were deemed to be similar. The maximum exterior girder distribution factors resulted from single and tandem truck crossings with one wheel line over the exterior girder (truck axle orientations d), e), and f)). These maximum distribution factors ranged from S/4.9 to S/5.6. The maximum measured girder distribution factor for the interior girders (truck axle orientations a), b), and c)) was S/6.7. As expected, truck speed was not a significant factor when determining girder load distribution factors. The super-position of truck axle orientations a) and b) from Figure 4 should also be investigating when considering maximum girder distribution factors. In the case of the maximum measured distribution factor for an interior girder (S/6.7), the denominator is reduced to 6.0 when these two axle orientations are combined.

Table 3a. Distribution Factor Results: Interior Girders (gray represents no data available)

Truck Axle Orientation (See Figure 4)	Speed (mph)	Oct. 2001				June 2002				October 2003			
		Strain		Deflection		Strain		Deflection		Strain		Deflection	
		avg	max	avg	max	avg	max	avg	max	avg	max	avg	max
a)	Idle	S/7.3	S/7.4	S/7.3	S/7.2	S/7.1	S/7.1	S/7.4	S/7.3	S/6.9	S/6.9	S/7.1	S/7.0
	15					S/7.0	S/6.9	S/7.5	S/7.4				
	25	S/7.7	S/7.4	S/7.6	S/7.5	S/7.3	S/7.2	S/7.4	S/7.2	S/7.0	S/6.9	S/7.1	S/6.9
	40	S/7.7	S/7.5	S/7.7	S/7.4	S/7.4	S/7.2	S/7.5	S/7.3	S/7.1	S/7.1	S/7.4	S/7.4
b)	Idle	S/7.5	S/7.5	S/7.5	S/7.5	S/7.2	S/7.2	S/7.8	S/7.7	S/7.4	S/7.3	S/6.8	S/6.7
	15					S/7.2	S/7.1	S/7.8	S/7.8				
	25	S/7.7	S/7.4	S/7.5	S/7.2	S/7.2	S/7.2	S/7.9	S/7.8	S7.5	S7.2	S7.0	S6.9
	40	S/7.7	S.7.5	S/7.8	S/7.7	S/7.2	S/7.2	S/7.7	S/7.7	S/7.5	S/7.4	S/7.3	S/7.0
c)	Idle	S/7.1	S/7.1	S/7.5	S/7.5	S/6.8	S/6.8	S/7.4	S/7.3	S/7.9	S/7.8	S/7.1	S/7.0
	15					S/6.9	S/6.9	S/7.4	S/7.4				
	25	S/7.2	S/7.1	S/7.8	S/7.6	S/6.9	S/6.9	S/7.4	S/7.4	S/8.0	S/7.9	S/7.9	S/7.3
	40	S/7.7	S/7.5	S/7.7	S/7.4	S/7.0	S/6.9	S/7.5	S/7.4	S/8.1	S/7.8	S/7.8	S/7.2
Max values for interior girders		S/7.1		S/7.2		S/6.8		S/7.2		S/6.9		S/6.7	

Table 3b. Distribution Factor Results: Exterior Girders (gray represents no data available)

Truck Axle Orientation (See Figure 4)	Speed (mph)	Oct. 2001				June 2001				October 2003			
		Strain		Deflection		Strain		Deflection		Strain		Deflection	
		avg	max	avg	max	avg	max	avg	max	avg	max	avg	max
d)	Idle	S/5.4	S/5.3	S/5.7	S/5.6	S/5.4	S/5.2	S/5.4	S/5.2	S/5.1	S/4.9	S/5.4	S/5.1
e)	Idle					S/5.2	S/5.1	S/5.2	S/5.2	S/6.2	S/6.2	S/5.8	S/5.7
f)	Idle					S/5.6	S/5.5	S/6.0	S/5.7	S/5.2	S/5.2	S/5.2	S/5.1
Max Values for exterior girders		S/5.3		S/5.6		S/5.1		S/5.2		S/4.9		S/5.1	

The AASHTO Standard Specification (AASHTO, 1996) and the AASHTO LRFD Specification (AASHTO, 1998) report girder distribution factors for timber deck/steel girder bridges as well as for timber deck/timber girder bridges. For comparison purposes girder distribution factors for glue laminated timber deck/steel girder bridges and glue-laminated timber deck/timber girder bridges were calculated and are shown in Table 4. Note that in the AASHTO Standard Specification the requirements for the two bridge types are identical.

Table 4. Comparison of Girder Distribution results with AASHTO Specifications

Girder	Maximum Measured	AASHTO Standard Specification	AASHTO LRFD		Infinitely Stiff Deck
			Timber Deck/Steel Girders	Timber Deck/Timber Girders	
Exterior	S/4.9	S/3.5 (Lever Rule)	S/3.5 (Lever Rule)	S/3.5 (Lever Rule)	S/14
Interior	S/6.7	S/4	S/4.5	S/5	S/14

The corresponding GDFs for multi-lane bridges are shown in Table 4 along with the maximum measured girder distribution factors for both an exterior girder and an interior girder. The interior girder distribution factor for the specifications vary from S/4 to S/5 and for exterior girders is determined by the lever rule which yields a girder distribution factor of S/3.5 for the Rt. 601 bridge. In addition, the transverse wheel load distribution for an infinitely stiff bridge deck (effectively a lower bound on the girder distribution factor) is given. This value is obtained by equally dividing the load between the girders and is S/14 for the Rt. 601 bridge.

The assumptions used in the design of the Rt. 601 bridge (girder distribution factors for interior and exterior girders for a glue-laminated timber deck-steel girder bridge from the AASHTO Standard Specification) were conservative and appropriate for use with this bridge as summarized in Table 4. Also, the AASHTO LRFD girder distribution factors for both exterior and interior girders were determined to be appropriate to use with this bridge as well. Based on the Rt. 601 field test results, a girder distribution factor of S/4.0 for interior girders and one from the lever rule for exterior girders is proposed for use with a glue-laminated timber deck over the 36 in DWB. These findings are in agreement with those for the Tom's Creek Bridge (Neely 2000) which supports there applicability to all glue-laminated timber deck-FRP girder bridges, however, more testing of similar bridges in-service is recommended.

Dynamic Load Allowance

A review by Paultre et al. (1991) on dynamic bridge behavior gives the calculation of a dynamic amplification of a passage of vehicles on a highway bridge as follows:

$$R_{dyn} = R_{sta}(1 + DA)$$

Where R_{dyn}= maximum dynamic response of the bridge

R_{sta}=maximum static response of the bridge

1+DA = Dynamic Amplification Factor

The AASHTO *Standard Specification* (1996) and the AASHTO *LRFD* (1998) refer to the dynamic amplification as the dynamic load allowance, or impact factor (DLA). Paultre suggests that full scale testing under normal traffic conditions is the most economical and practical means to evaluate dynamic amplification (1992). Determining the impact factor from field testing, the equation is rearranged for the dynamic load allowance as follows:

$$IM = \frac{R_{dyn}}{R_{stat}} - 1$$

Eq. 4

Where R_{dyn}= maximum dynamic response
of the bridge (strain or deflection)

R_{sta} = maximum static response
of the bridge (strain or deflection)

IM = Dynamic Load Allowance

The dynamic behavior of the Rt. 601 Bridge was investigated using the strain and deflection results from a series of dynamic load tests performed in October 2001, June 2002. and October 2003. Peak responses at mid-span from both strain and deflection data were used in the calculation of the dynamic load allowance. Static and dynamic responses used in the calculation were values obtained from identical truck axle orientation with the only difference being truck speed. The idle speed crossings were used as the static condition, and the faster speeds from 15 mph, 25 mph, and 40 mph were used to represent dynamic conditions. Strain versus time of a typical static pass and a 40 mph truck pass are compared in Figure 6.

The first step in the calculation procedure involved isolating the five static runs and obtaining average static strains and deflections for each girder. This average static value would be used for the R_{static} variable in Eq. 4. Each dynamic response was substituted in the R_{dyn} numerator, with five dynamic load allowances calculated for each axle orientation test for each truck speed.

$$IM = \frac{\mathcal{E}_{dynamic}}{\mathcal{E}_{static}} - 1$$
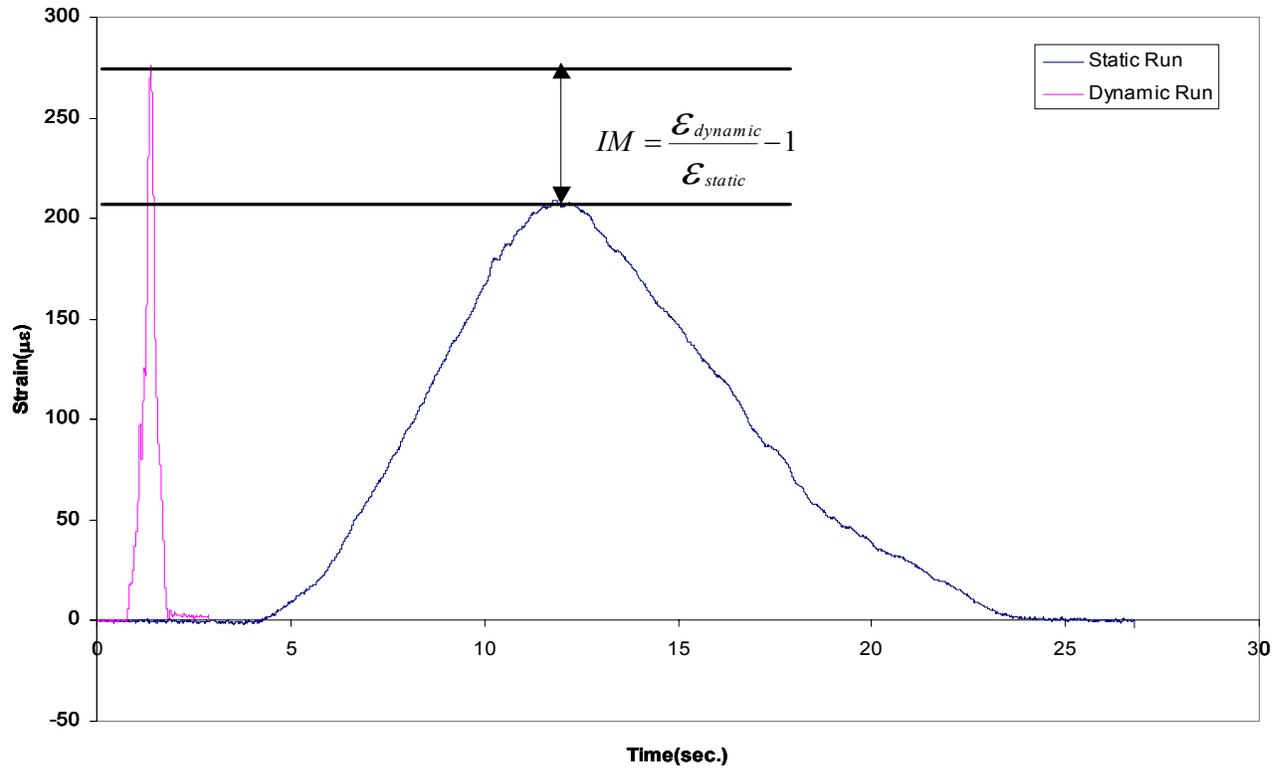
Figure 6. Typical Rt. 601 Bridge girder response due to truck loads with static and dynamic results superimposed.

Dynamic load allowances were calculated at all girders for each dynamic truck pass, but only the girder with the maximum response was taken into consideration for determining the dynamic load allowance for the bridge system. A dynamic load allowance from five repetitions of truck passes were calculated for the three truck axle orientations considered ((a), b), and c) in Figure 4). For the October 2001 field test, only 25 mph and 40 mph truck speeds were conducted for dynamic testing. A total of six different average and maximum dynamic load allowances were calculated for the October 2001 by taking into consideration the three different axle positions at two different dynamic speeds. For the June 2002 field test, an additional speed of 15 mph was added to the testing sequence; therefore, nine sets of average and maximum dynamic load allowances were calculated. The October 2003 field test was essentially the same as the one performed in October 2001. The maximum and average dynamic load allowances for the three live load tests are shown in Table 5.

Table 5. Measured Dynamic Load Allowance Summary in Percent. Results are based on maximum girder strains and deflections (gray represents no data available)

Truck Axle Orientation (see Figure 4)	Speed (mph)	October 2001				June 2002				October 2003			
		Strain		Deflection		Strain		Deflection		Strain		Deflection	
		avg	max	avg	max	avg	max	avg	max	avg	max	avg	max
a)	15					7.8	9.8	4.6	6.6				
	25	10.1	13.8	6.5	8.9	3.8	4.1	2.6	3.2	1.9	6.9	0.6	3.3
	40	4.3	6.7	0	4.4	-1.0	7.1	5.7	12.8	11.3	16.1	14.4	19.1
b)	15					3.9	6.6	2.3	3.0				
	25	7.2	13.5	6.0	9.3	8.7	9.7	7.4	8.2	2.2	0.3	-0.2	6.2
	40	-2.6	1.8	1.5	3.8	29.4	31.6	28.4	30.4	10.0	3.8	0.5	3.3
c)	15					6.8	8.3	0	1.7				
	25	-1.0	11.7	-4.0	0	7.7	8.0	5.4	7.1	2.8	6.5	-3.1	-0.8
	40	-7.6	-3.4	-6.6	-3.8	23.0	35.7	21.6	27.1	-1.9	1.6	3.9	9.4

Dynamic Load Allowance Results: October 2001 Test

The magnitude of the dynamic load allowance in the October 2001 live load tests for both the 25 mph and 40 mph truck crossings were comparatively small. The DLA values in Table 5 show the DLA for the truck crossings were generally higher for the 25 mph live load test than for the 40 mph live load test. Also, the dynamic load allowances reported in Table 4 for the October 2001 live load test are well below the assumed DLA of 30 %.

Some conclusions were drawn from the evaluation of the October 2001 dynamic load allowance results. Paultre et al (1992) considered vehicle speed to be an important factor in determining the dynamic amplification phenomenon. He suggests that increasing speed of a vehicle should increase dynamic load amplification but that lower bridge responses from the increased test speeds can be caused by several factors with bridge approaches being a major factor.

The Rt. 601 bridge experienced settlement at both approaches shortly after construction and before the first live load test in October 2001, as a result of inadequate compaction of the soil back fill toward the abutment ends. Settlement on the order of 1 in or more ensued on both approaches, creating a non-ideal condition at the approaches. Many highway bridges use approach slabs to prevent excessive settlement at the approaches, but for bridges on rural roads the use of approach slabs is not practical due to the low amount of traffic and the cost associated with construction of approach slabs.

It is believed that the settlement at the approaches caused the truck to ramp over the bridge. The ramping effect increased with the speed of the test trucks. A similar phenomenon occurred during testing of the Washington School House Lane Bridge in Cecil, Maryland (STI, 1998). Structural Testing Incorporated (STI) reported that some strain readings on the FRP composite slab bridge from static runs were higher than the truck runs at higher speeds. They attributed this behavior of a negative dynamic load effect to a combination of a short span and the varying contours at the approaches of the bridge.

After the October 2001 live load test an attempt was made by the Virginia Department of Transportation to level the approaches by filling the settled areas with asphalt. The repaired approaches with the repaired areas having the darker asphalt are shown in Figure 7. The second live load test in June 2002 took place with the improved approaches. To further investigate the effect of settlement, an additional speed of 15 mph was used for the June 2002 live load test to further investigate how slower speeds affect dynamic load allowance of the bridge.

Figure 7. Improved Approaches during June 2002 field test.

Dynamic Load Allowance Results: June 2002 Test

The effect of the improved approaches can be seen in the dynamic load allowance results for the Jun 2002 live load test in Table 5. For the truck crossings with axle positions a) and c) more typical bridge dynamic behavior was seen. The DLA increased with increasing truck speed, especially when the speed increased from 25 mph to 40 mph. The maximum measured dynamic load allowances were approximately equal to the assumed value of 30 %.

For the truck crossing with axle orientation b) similar behavior to that experienced during the October 2001 live load test was seen. The measure dynamic load allowances were small and some negative dynamic load allowances were recorded. This behavior is believed to be due to the condition of the approaches again. Even though an attempt had been made to level the approaches there was still some settlement. This settlement was in the approaches as the truck crossed the bridge in axle position b), hence the smaller dynamic load allowances.

19

Dynamic Load Allowance Results: October 2003 Test

For the October 2003 field tests the effect of the improved approaches was still noticeable but there appears to have been further settlement of the approaches. The DLA results for October 2003 are essentially bracketed by the October 2001 and June 2002 results.

Comparison of Dynamic Load Allowance Results

The maximum dynamic load allowance results from the three live load tests are compared with those from the AASHTO Standard Specification and AASHTO LRFD in Table 6. The maximum results from the June 2002 live load test were in close agreement with, but slightly greater than, the AASHTO Standard Specification value of 30% (the value used in design) and AASHTO LRFD value of 33 %. The dynamic load allowance for all wood bridges or wood components of bridges is much less than that given above. The smaller dynamic load allowances for these types of wood bridges were not used in the comparisons since the concern here is the behavior of the Dickey Creek Bridge superstructure system which is not all wood.

Table 6. Summary of Dynamic Load Allowance Results

Test Date	Maximum Measured DLA from Strain Measurements (%)	Maximum Measured DLA from Deflection Measurements (%)	AASHTO Standard Specification DLA (%)	AASHTO LRFD DLA (%)
October 2001	13.5	9.3		
June 2002	35.7	30.4	30	33
October 2003	16.1	19.1		

The maximum results from the October 2001 live load test were significantly less than the design values for the reasons discussed previously. The proposed dynamic load allowance for a glue-laminated timber deck-FRP girder bridge similar to the Rt. 601 bridge is 50 %. This recommendation is 40% greater than the maximum measured DLA from the field tests (35.7%). This cushion is necessary to allow for statistical variations in the results.

For the Tom's Creek Bridge a maximum dynamic load allowance of 90 % was recorded (Neely 2000) indicating that the dynamic load allowance for bridges with smaller FRP girders or at shorter spans can be considerable higher than that measured for the Rt. 601 bridge. Since major factors affecting dynamic load allowance are the condition of the bridge approaches and truck suspension it is recommended that testing of other glue-laminated timber-FRP girder bridges with varying sizes of FRP girders and girder spacings be conducted before developing recommendations for all such bridges.

Service Load Deflections

A summary of the measured deflections from the Rt. 601 bridge during the three live load tests is shown in Table 7. It is apparent that the deflection of the Rt. 601 bridge increased from October 2001 to June 2002 under similar truck and axle orientations. The increase ranged from 10 to 50 % for similar truck axle orientations and averaged 22 %. It can be seen from comparing the deflection results from June 2002 to October 2003 the deflection of the bridge decreased about the same amount from the June 2002 to the October 2001 field test (average decrease was 23%). The general increase and then decrease in deflection over time can be attributed to several reasons:

1. The test trucks for the June 2002 live load test weighed slightly more than for the October 2001 and October 2003 live load tests.
2. Loosened connections between the timber deck and girders which provided a small amount of composite action may have contributed to the increased flexibility of the bridge system.
3. Warmer temperatures during the June 2002 live load test may have contributed to the larger girder responses. The average daily mean ambient air temperature for the June 2002 test was 79ºF (22ºC), compared to 54ºF (15ºC) for the October 2001 test and 50ºF for the October 2003 test. The Tom's Creek Bridge live load tests experienced similar behavior in that larger responses resulted from spring and summer tests conducted at higher temperatures (Neely 2000).
4. As a result of higher temperatures in the June 2002 test, a change in the thermal properties of the neoprene bearing pads may have contributed to higher girder deflections.

Table 7. Deflection Summary of October 2001 and June 2002 field tests (gray represents no data available)

Truck Axle Orientation	Speed (mph)	October 2001 Deflections (in)		June 2002 Deflections (in)		October 2003 Deflections (in)	
		max	avg	max	avg	max	avg
a)	Idle	0.209	0.209	0.252	0.240	0.220	0.200
	15			0.252	0.240		
	25	0.209	0.201	0.272	0.260	0.206	0.201
	40	0.201	0.201	0.311	0.299	0.238	0.228
b)	Idle	0.201	0.189	0.228	0.220	0.195	0.193
	15			0.240	0.228		
	25	0.209	0.209	0.240	0.228	0.205	0.193
	40	0.201	0.201	0.240	0.240	0.200	0.194
c)	Idle	0.220	0.209	0.240	0.240	0.187	0.187
	15			0.252	0.252		
	25	0.240	0.228	0.272	0.260	0.185	0.181
	40	0.220	0.220	0.311	0.311	0.204	0.194
d)	Idle	0.272	0.260	0.319	0.311	0.256	0.252
e)	Idle			0.319	0.311	0.216	0.211
f)	Idle			0.291	0.280	0.256	0.254

The small deflection increase with higher temperatures on tests days is in agreement with the results reported by Neely (2000). He noted that the response of the Tom's Creek Bridge due to vehicular loading appeared to be related to ambient air temperature. Neely also noted that the increased deflections seen in the Tom's Creek Bridge during live load tests on warm days were temporary with the bridge experiencing lower live load deflections on succeeding live load tests on cooler days.

For the October 2001 test, the maximum deflection occurred from truck axle position d) with the outside wheel lines of the two trucks aligned over the centerline of the exterior girders. The maximum average deflection was 0.26 in, which is equivalent to L/1800. The multiple lane test (axle orientation d) was performed again during the June 2002 field test. The maximum average deflection was 0.31 in, a 12% increase from the October 2001 test. The multiple lane runs were only performed at idle speeds for both field tests, thus dynamic effects are not taken into account. Applying the proposed dynamic load allowance of 50% (discussed previously) to the multiple lane deflections, the October 2001 maximum deflection was 0.39 in (L/1200) and the June 2002 was 0.47 in (L/996). The maximum measured deflection (L/996) is about 25 % less than the design deflection target of L/800.

The increased stiffness observed in the constructed bridge over the design expectations of Waldron (2000) point to the contribution of elements other than girders. Stallings and Yoo (1993) reported that field testing results can reveal a hidden amount of reserve stiffness from secondary elements. One area that contributes extra stiffness to a bridge system is unintended partial composite action in bridges that are not constructed with shear studs or other shear transfer devices. Partial composite action can result from partial shear transfer between the deck and top flanges, thus shifting the neutral axis of the bridge and lowering the maximum moment. Support conditions can also contribute to extra stiffness of a bridge system. For simply supported beams, frictionless supports are assumed. However, when truck loads are applied on a bridge, the ends of the girders rotate in a manner that causes the bearings to move away from mid-span. Restraining moments are then caused by the frictional forces at the bearings, which reduce the bending moment resisted by the girder along the span. In addition to bearing restraint, other elements such as guardrails and diaphragms can stiffen the edge of a deck and resist moment as well. The main point is that a three dimensional structure does not resist loading the same as a set of one dimensional beams (Stallings and Yoo, 1993), thus contributing to the discrepancy between calculated and measured girder deflections.

The discrepancy in observed performance as compared to the predicted performance derived from the design may also lie in the differences between the design truck and test trucks. The Rt. 601 Bridge was designed using AASHTO HS-20 loading, where three truck axles of 8 kips and a pair of 32 kips are used. The dump truck used in the June 2002 field test had a 14.2 kip front axle and a pair of 20.6 kip rear axles. When the loads (with girder distribution and impact factors applied) are placed at the position to provide the maximum moment on a simply supported beam, the load effect of the AASHTO HS-20 is approximately 11% more than the test truck, thus contributing to the deflection difference. The three axle dump trucks were used because of weight restrictions of other adjacent bridges in Sugar Grove, availability, and ease of loading the dump truck to give significant load effect. Furthermore, the truck gives more of a true representation of the maximum load effect that the bridge can expect to experience during service.

Effect of Diaphragms

The three interior diaphragms near mid-span were removed between girders five and eight during the June 2002 live load test to investigate the function of and necessity for interior diaphragms. End diaphragms at the support and the remaining interior diaphragms between girders one and five remained in place. Mid-span girder deflections and strains were recorded for five passes at creep truck speed with axle orientations a) and e). Strains and deflections in girders five through eight were generally higher with the mid-span diaphragms removed. The higher responses resulted in increased distribution factors for the most heavily loaded girders. Consequentially, this resulted in decreased girder distribution factors in girders one through four.

Barr et al (2001) investigated the effects of diaphragm removal on girder distribution using a finite element model for prestressed I-girder bridges. The removal of diaphragms in the model resulted in slight increases in girder distribution. A study performed for the Alabama Department of Transportation (Stallings 1996) of steel girder bridges with diaphragms reported field test results of bridges with and without diaphragms. The goal of the study was to investigate the effects of fatigue cracking at diaphragm to girder connections, and to eliminate such connections where fatigue cracking was a problem. Field tests were conducted before and after all interior diaphragms were removed. Interior diaphragms are diaphragms located along the bridge span in between the supports, but did not include the diaphragms at the support. Interior girder stresses determined from field tests and a finite element analysis increased approximately 15% with the removal of diaphragms.

Girder distribution factors for the heaviest loaded girders with and without interior diaphragms between girders 5 and 8, are shown in Table 8. The maximum increase in girder distribution factors was 12.3 % for an interior girder and 7.8 % for an exterior girder. Although not included in Table 8, the magnitude of girder strains and deflections increased by 8 and 12 % for the most heavily loaded girders. The increase in girder distribution stresses, deflections, and distribution factors were similar to that reported by Stallings (1996). The increase in girder distribution factors for the Rt. 601 Bridge is negligible when compared to the difference between the recommended girder distribution factors and the maximum measured values shown in Table 4.

Table 8. Comparison of Girder Distribution Facotrs With and Without Interior Diaphragms

	Truck Axle Orientation a)		Truck Axle Orientation e)	
	From Strain Measurements	From Deflection Measurements	From Strain Measurements	From Deflection Measurements
With diaphragms	S/7.7	S/8.1	S/6.3	S/9.1
Without diaphgrams	S/6.9	S/7.7	S/6	S/8.5
Percent Increase (%)	12.3	5.1	5.4	7.8

Physical Condition of the Rt. 601 Bridge

The Dickey Creek Bridge has been visually inspected periodically since the bridge was opened to traffic. The bridge was judged to be in very good condition at the time of opening. Up until inspections performed during the Fall of 2003, there were no signs of deterioration of the FRP double web beams due to environmental exposure, creosote from the timber deck, or from fatigue due to repeated traffic crossings. However, the asphalt wearing surface did have a few small reflective cracks.

During inspections performed during the Fall of 2003 and the Summer of 2004 some deterioration or damage of the FRP beams was discovered (Kassner 2004). The three types of deterioration/damage found (splinters, blisters, and cracks) will be described in detail below. It is important to note that the deterioration/damage found during the Fall 2003 inspection was present during the October 2003 live load test. The results of this live load test show no changes in behavior that can be attributed to the deterioration/damage found. The type and extent of the deterioration/damage is well documented (Kassner 2004) and should be periodically monitored to insure this is not progressive behavior.

With regard to the "splinters," they ranged in length from 1.5 in. to 12 in. long, with Girder 5 exhibiting the most extensive amount of this type of deterioration or damage. Typically, these splinters were about $^1/_8$ in. to $^1/_4$ in. wide, and in some cases, the splinters were still attached to the beam. Figure 8 shows a typical splinter from the bridge. These splinters appear to consist only of the resin matrix material. However, in some cases, the carbon fibers were exposed. About two-thirds of the splinters occur within 4 ft of midspan; the others range from 5 ft to 9 ft away from the ends of the beams. All splinters found were on the bottom flange. Apart from the ten splinters found during the Fall 2003 inspection, five additional splinters were discovered in the Spring of 2004. One splinter is along the downstream side of Girder 1, a second has been found near midspan on the upstream side of Girder 5, another is on the upstream side of Girder 6, and the remaining two are along the downstream side of Girder 7. There is the possibility that these additional splinters were present but not noticed during the prior inspection.

While there does appear to be a couple of locations where damage occurred in Girders 1 and 5, the number of splinters in all of the beams is evenly split between being located on the upstream side of a girder versus the downstream side. Therefore, there is no conclusive evidence that this splintering effect is strictly due to damage from debris floating downstream during a high-water event. Furthermore, there was very little debris on top of the abutment or in between the girders, which again suggests that local flooding did not reach the girders.

Since a third of the splinters occur closer to the ends of the girders, there is only a small likelihood that the splintering was due to moment induced stresses at midspan. Besides, the failure mode that Waldron (2001) observed while loading a beam to failure was one of delamination between the carbon fiber and glass fiber interface in the *top* flange, not in the bottom flange, which is where most of the splintering has occurred in the Route 601 Bridge.

Figure 8. Matrix resin material splintering off from Girder 5 of the Route 601 Bridge

Ruling out the two aforementioned reasons behind the splinters leaves open the third possibility of construction damage that might have occurred while setting the beams in place. The splinter on the bottom of the top flange 6 ft (1.8 m) away from the west end of Girder 7 supports this theory. Representatives from Strongwell Corporation have also suggested that these splinters may actually be flaws due to production errors, where the fibers may have been set too close to the edge of the flange. If this theory were in fact true, then there would be an alarming rate of production flaws considering that four of the eight beams used in the Route 601 Bridge had splinters in them. Regardless of the reason, the splintering issue is one that needs continued monitoring to see if the splinters grow or any additional splinters appear. As noted before, the splinters discovered during the Fall 2003 inspection did not appear to increase in length.

The other previously mentioned problem is the "blisters" on the bottom flanges of the two exterior girders, i.e., Girders 1 and 8. Figure 9 shows a typical blister found on the girders. These blisters measured 1 in. to 3 in. in length, and appeared close to both the upstream and downstream edges of the bottom surface of the bottom flange. During the Fall 2003 inspection, these blisters were only noted on the western half of the two beams. However, the Spring 2004 inspection revealed a 1 in. blister located 4 ft east of midspan in Girder 1 and a set of blisters extending 26 in. east of midspan in Girder 8. Additional blisters were discovered about 3 ft away from the west end of Girder 8, as well as 20 in. beyond the extent of the original set of blisters in Girder 1 during the Fall 2003 survey.

**Figure 9. Typical blister on the surface of the bottom flange in an exterior girder
for the Route 601 Bridge.**

The blisters were "hard" and could not be pressed inward with any degree of thumb pressure. Soundings taken by bouncing a quarter on the top of the bottom flange above the blistered area appeared normal versus unaffected FRP material. The same was true when tapping directly on the blisters. These soundings suggest that little if any delamination has occurred in these areas. Because the blistering occurred only on the two exterior girders, the primary suspect for the blistering is water intrusion. The fact that more blisters occurred on the exterior portion of the girder than the interior half helps to support this hypothesis, since the exterior half of the beam has greater exposure to water and moisture, thus is more prone to water intrusion. As previously mentioned, the blisters that were originally discovered during the Fall 2003 survey did not appear to have grown in size in the subsequent examination. Nevertheless, these blisters need continued monitoring in assessing the long-term viability of FRP in service conditions.

One problem that was not noticed during the Fall 2003 inspections is the presence of several longitudinal "cuts" in the surface of the bottom flange in several girders. These cuts appeared to be just that or like a deep scratch, rather than a crack; they had a constant thickness and remained straight along the length of the beam. Both Girders 5 and 6 exhibited a single cut along the full length of the beams. Girder 6 had an additional cut that was about 5 ft long starting at the east end of the beam. Likewise, Girder 7 had a cut that was 25 in. long at the east end of the beam. While the cuts did not appear to be the result of deterioration, future surveys should measure their length and thickness in order to ensure that the cuts are not growing beyond the initial damage.

26

Assessment of 36-inch DWB Strength & Failure Mode

Capacity and Failure Mode

Following the Tom's Creek Bridge rehabilitation, a number of the 8 inch double-web beams were tested to failure (Hayes 1998). As tested in three- and four-point bending, the 8 inch DWB consistently failed within the compressive flange at a primary interface between carbon and glass fibers. The failure was considered to be delamination, given the low strains measured on the flange at failure and the consistent location of the separation. Furthermore, the delamination appeared to initiate in the vicinity of the load patches, indicating a stress concentration effect. Schniepp (2002) and Hayes (2003) tested 19 36-inch DWBs to failure under four-point bending (Figure 10). Again, the failure mechanism appeared to be delamination within the compressive flange (Figure 11), initiating at the load patches. As in the case of the 8 inch DWB, the failure occurs at relatively low in-plane strains, suggesting that the delamination caused premature failure prior to compression failure. Likewise, in both the 8 and the 36-inch DWB the shear capacity exhibited a dependence on span (span-to-depth ratio specifically) as shown in Figure 12.
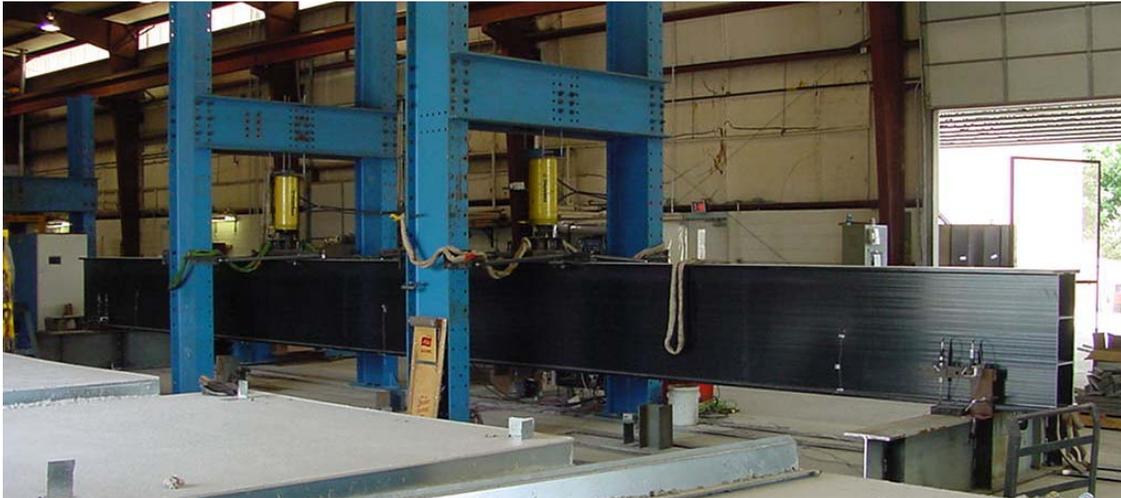
Figure 10. Four-point bend test set-up for 36 inch DWB (18.3 m or 60 ft span shown).
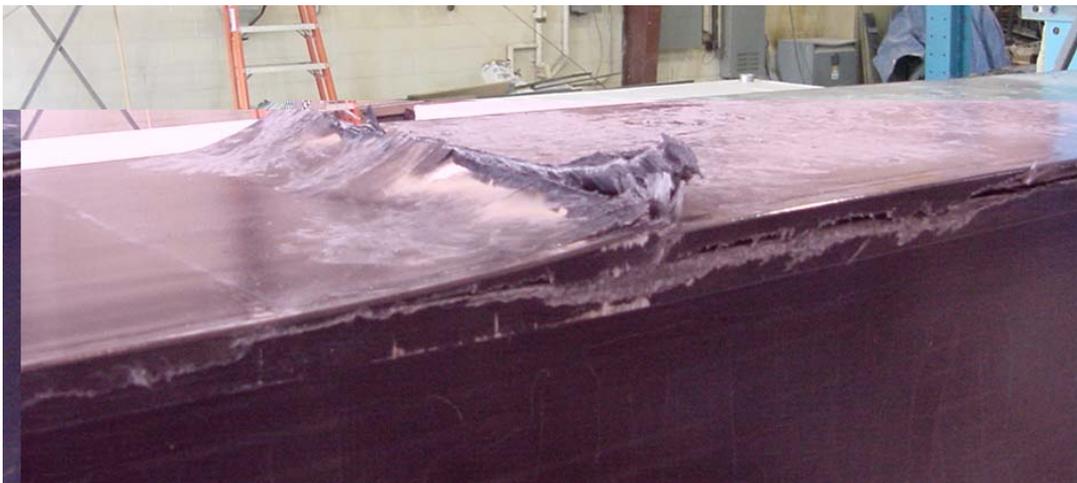
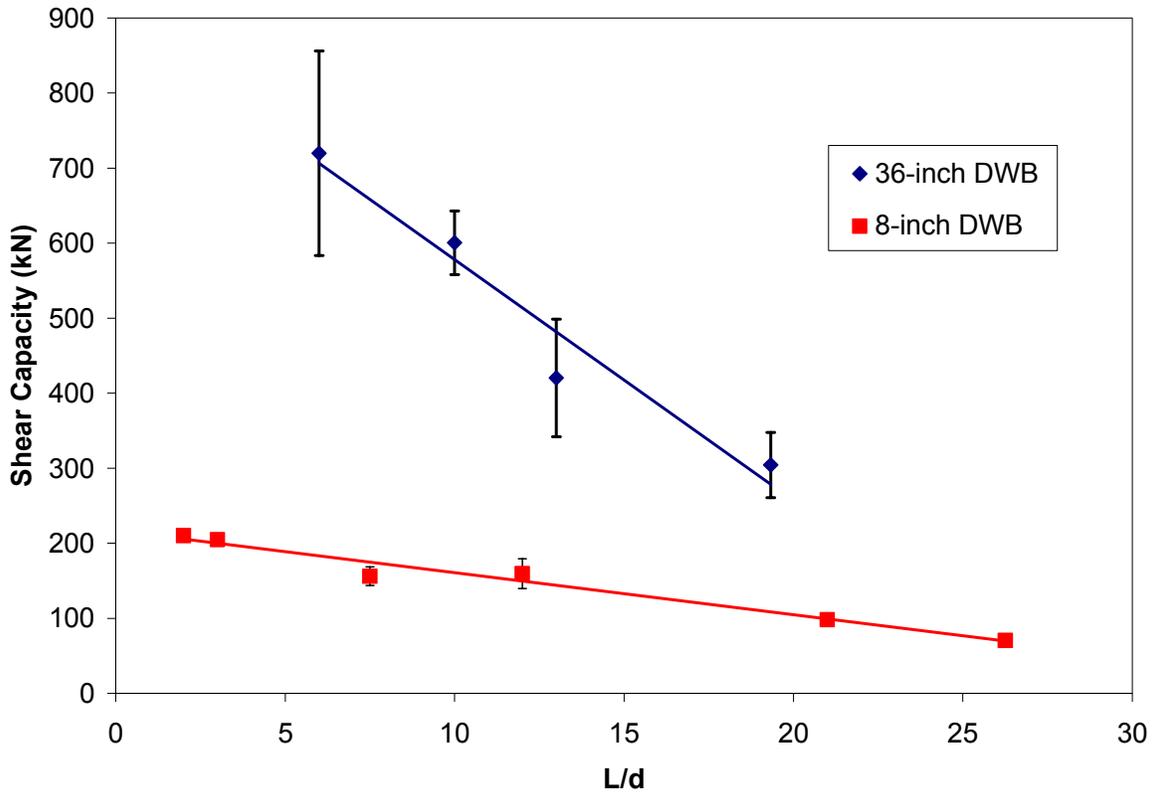**Figure11. Failure of the compressive flange of a 36 inch DWB under the loading patch.**

Figure 12. Span dependence of the shear capacity for both the 8 inch and 36 inch DWBs.

The lay-up of the 36 inch DWB is proprietary, but the flange can be represented as two sub-laminates as shown in Figure 13. The outer sub-laminate essentially consists of alternating layers of unidirectional carbon tows and glass fiber continuous strand mat (CSM), while the inner sub-laminate is formed from half of the web material and is basically a quasi-isotropic lay-up of glass fibers only. Although the intent in the final structure was to uniformly position each of the plies within the section, the reality of the processing leads to non-uniform distribution of fiber tows and plies as shown in Figure 14. Possible delamination initiation sites include the free edge or the inner flange taper at the interface between the two sub-laminates, where the innermost carbon ply is adjacent to a [0/90] glass fabric (see Figure 15). The problem of delamination at material and geometric discontinuities such as free edges and tapers is well known and was studied in an effort to describe the initiation of damage and failure of the beam.
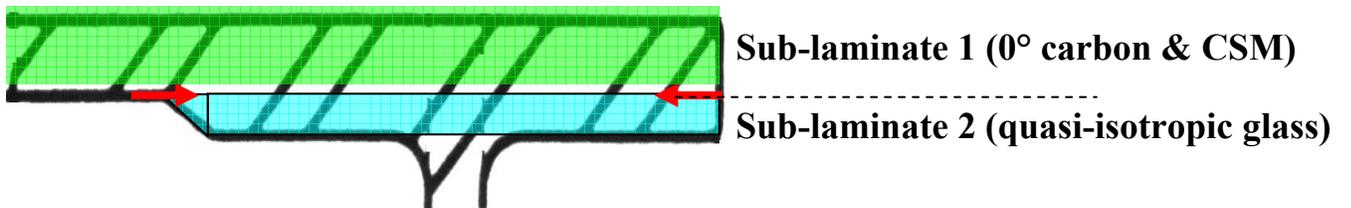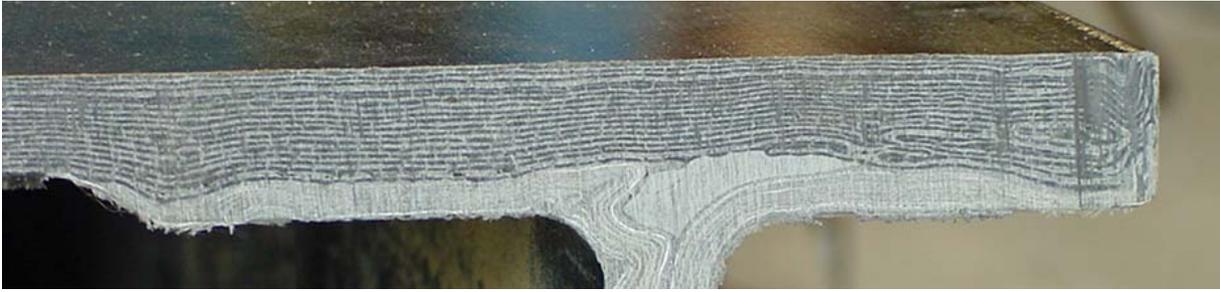

Sub-laminate 1 (0° carbon & CSM)

Sub-laminate 2 (quasi-isotropic glass)

Figure 13. Sub-laminate construction of the DWB's flange. Arrows indicate possible delamination sites.

28

Figure 14. End view of DWB showing lay-up detail on both sides of flange.

Figure 15. Possible delamination at the taper in two different beams. (Samples taken from near the end of the delamination.)

36-inch DWB FEA Modeling for Strength

Half-beam models of the DWB under four-point loading geometry for spans of 18, 30, 39, and 58 ft were constructed in ANSYS$^{®}$, employing symmetry conditions at mid-span to reduce the number of elements (Figure 16). The end constraints were modeled by simply specifying zero displacement at the end nodes on the bottom edge of the beam, since the stresses at the end supports are not important for these spans. The 3-D 8-noded layered brick SOLID46 elements were used to model the walls of the beam. The beam was meshed with 3 inch long elements in the *x*-direction, but in the region under the pad and one pad width on either side of the pad, the mesh was refined further (0.5 to 1 inch long elements) to properly capture stress gradients. The model was solved for two values of the change in temperature following cool-down from cure: $\Delta T = 0$ and $\Delta T = 75\ °F – 280\ °F = -205\ °F$. The first case neglects residual thermal stresses, and the second case models full thermal effects, assuming a cure temperature of 138 ºC (280 °F) and a lab test temperature of 75 °F.
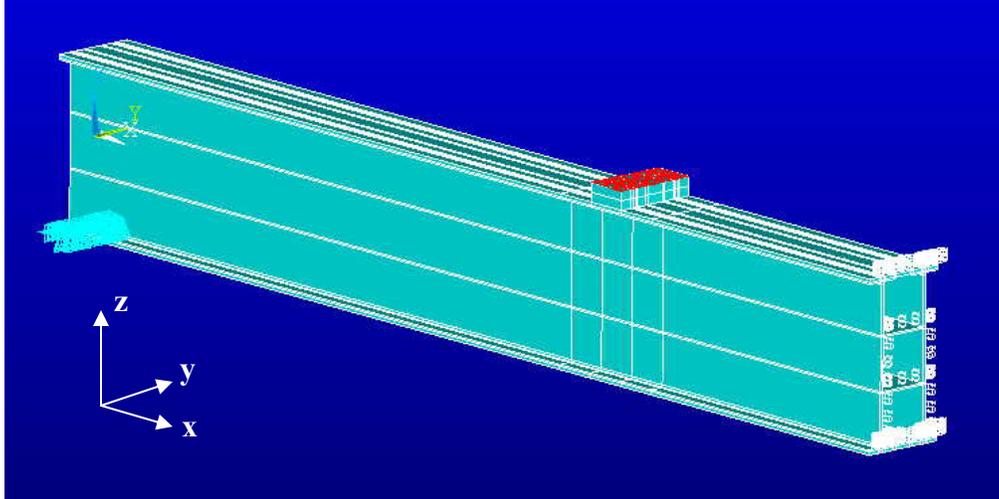
Figure 16. Half-beam model used in FE global analysis (11.9 m span).

The deflection at mid-span on the bottom flange was checked for agreement with the experimental values and (Modified Laminated Beam (MLB) theory and good agreement was achieved. The predicted in-plane stresses and strains through the depth of the flange at mid-span were also compared with the MLB prediction, assuming no residual stresses due to processing, i.e. $\Delta T = 0$. Again these predicted stresses compared well between the two methods.

Using the sub-modeling feature in ANSYS®, a sub-model at the free edge was developed (Figure 16). The free edge was idealized with perfectly flat and uniform plies. This is a significant oversimplification of the actual beam cross-section shown in Figure 14 which shows significant ply waviness and variability in the vicinity of the free edge. Nevertheless, identifying and modeling a more realistic lay-up/construction that is common to all manufactured beams would be extremely difficult. Furthermore, the nature of the free edge is likely to vary across different production runs. The idealized model provides a simplified means to predict strength and investigate the sensitivity of the interlaminar stresses to loading conditions and beam construction.

The procedure actually consisted of two sub-modeling steps. In the first step, a 9 inches long by 2.5 inches section of the top flange centered at the edge of the pad was modeled (EDGESUB1 in Figure 16). Thus, half the sub-model is under half of the load patch, and half is outside the patch. The pad and plate volumes and the applied pressure on the steel plate were included. EDGESUB1 was meshed using the SOLID46 3-D element, but each ply was modeled as a single layer of elements.

In order to provide additional refinement at the free edge, where gradients in stress are known to be very large, a second sub-model, EDGESUB2 (not shown), was constructed. This sub-model (shown in Figure 17) was a 1 inch x 1 inch x 1.032 inch volume to be centered along the free edge at the location of interest, the region modeled using EDGESUB1. Each ply was modeled using individual SOLID191 elements, the quadratic version of the SOLID46 element to obtain more accuracy with the same number of elements. The cut boundary nodal interpolation procedure above was repeated, using the results of EDGESUB1 as the input for EDGESUB2.

30
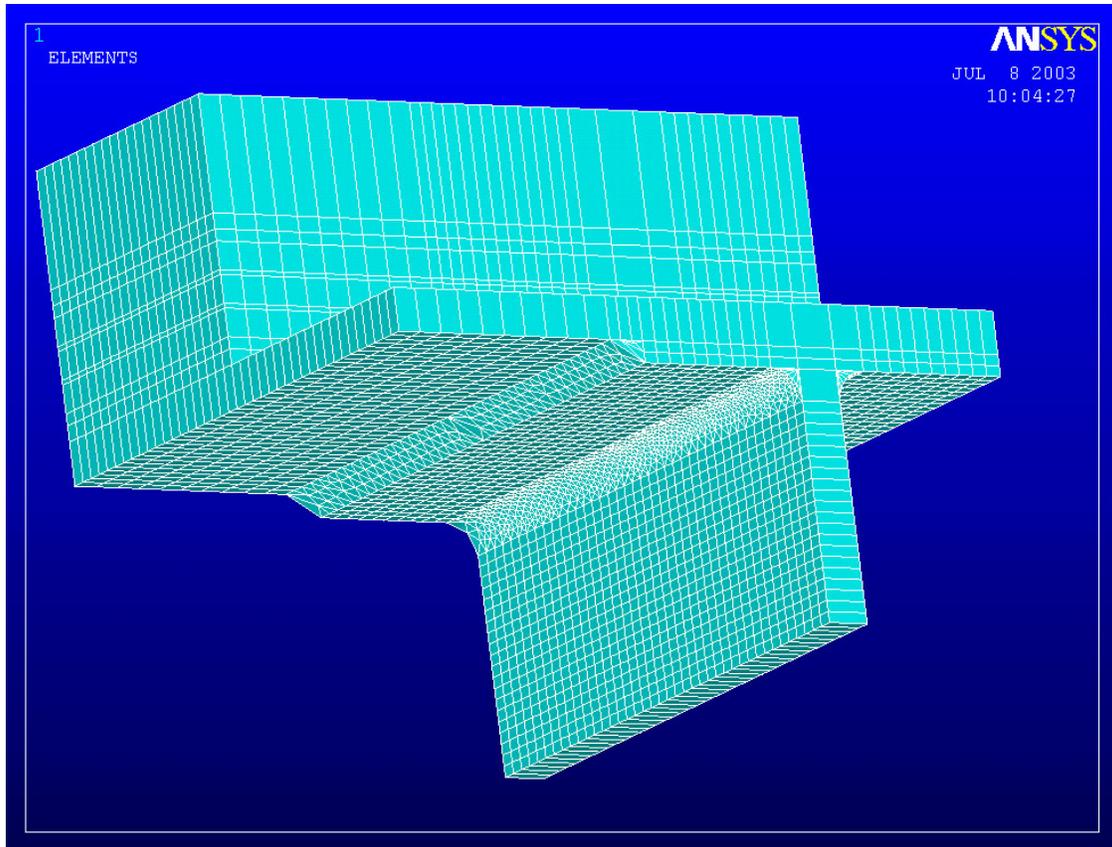
Figure 17. Intermediate FE submodel (EDGESUB1) used for the taper region stress analysis.

These models were used to compute the local stresses at ply interface as well as within plies and compared against the appropriate failure criteria. We examined the interlaminar shear stress at both the free edge and interior flange taper. When comparing the predicted failure load given various interlaminar failure criteria, it was determined that a shear-induced failure might not be what is controlling the failure, as shown in Figure 18. There is poor agreement between the observed shear capacity as a function of span and that predicted for the taper edge delamination failure mode using the ply width stress averaging technique (Hayes 2003).

Reexamining the in-plane stress and considering the possibility that the controlling or first failure was controlled by compression, these in-plane stresses were compared to measured compression strengths for coupons extracted from the DWB flange. End loaded side supported compression testing revealed a lower than normal strength of 75.1 ksi for the predominately carbon/vinyl ester section of the flange. When compared with the predicted in-plane stresses from the FEA sub-modeling it suggests that compression strength of the flange controlled the failure of the 36-inch DWB, as shown in Figure 19.
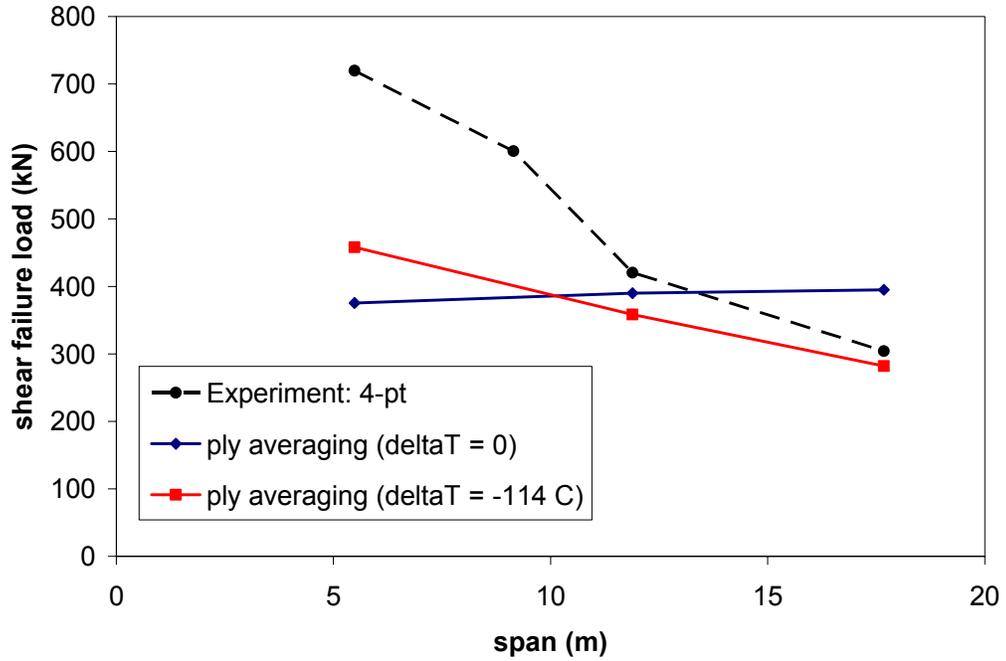
**Figure 18. Comparison of the predicted shear capacity vs. span length for
the taper edge delamination failure mode using the ply width stress
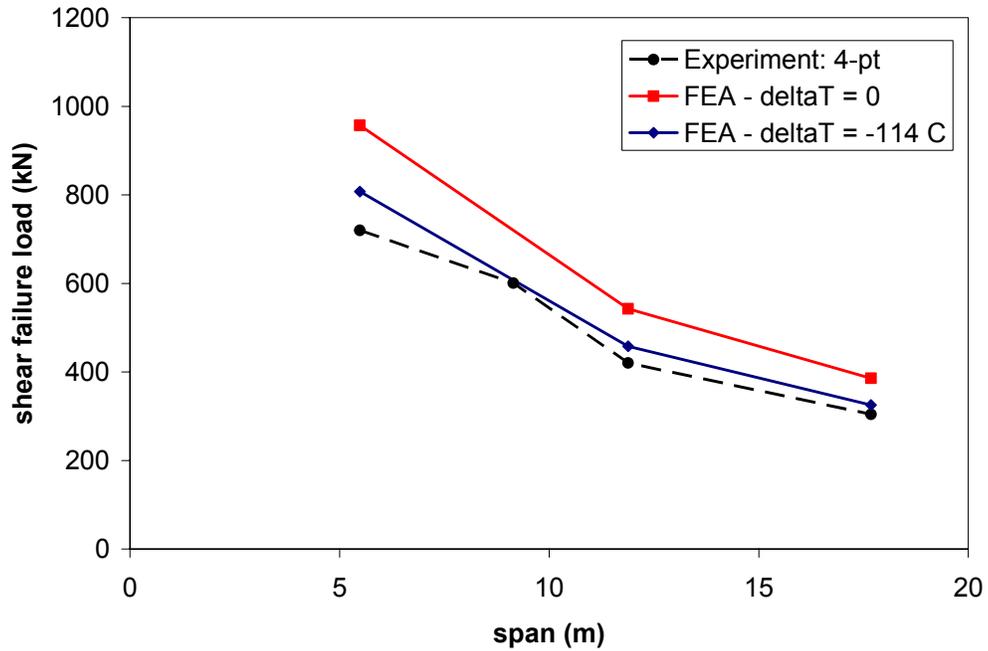averaging technique and the experimental results.**

**Figure 19. Comparison of the predicted shear capacity vs. span length for the compressive failure mode and
the experimental results.**

An approach similar to that of Senne (1999) was followed to develop fatigue life predictions. However, based on the evidence suggesting that the failure mode is compression failure of the carbon plies, the delamination analysis was not utilized. The finite element stress analysis developed in the previous sections was integrated into a code that accounts for stiffness reductions with cycles due to matrix cracking in the off-axis plies of the tensile flange. Shear stiffness reduction in the web panels were not considered due to the relatively low shear strains observed and the limited effect that the web performance has on the flange stresses. Empirical expressions for the stiffness reduction were taken from glass/vinyl ester coupon data. The remaining strength of the carbon fiber critical element was tracked using the critical element model of Reifsnider and Case (2002). Finally, fatigue predictions were generated for the 36 inch DWB at various load/stress levels. These predictions were then compared to results from two full-scale fatigue tests.

The ANSYS® Parametric Design Language (APDL) was used to automate the global model solution and post-processing employed in the stress analysis and failure prediction. The analysis was then inserted into a DO-LOOP structure, in which the cycle count n is incremented by a user defined amount, Δn. During each cycle, the critical element is checked for failure by comparing the remaining strength to the applied loading (failure function). If failure occurs, the code stops. Otherwise, the stresses in the off-axis plies are checked for failure and then discounted or degraded according to stiffness reduction curves specified by the user. The entire process is repeated until ultimate failure occurs. Further details of this analysis can be found in Hayes (2003).

The resulting fatigue life curve for the 39 ft four-point test geometry is shown in Figure 20. The results suggest that at the 30 kip load level, failure is predicted to occur at 4.4 million cycles, while the experimental test (indicated as a run-out in the figure) was stopped 4.9 million cycles with no signs of damage. Failure is predicted to occur at 32,000 cycles for the 81.6 kip load level; the testing is incomplete. The fatigue test at this load level resulted in a longitudinal flange splitting and was stopped after 100,000 cycles due to the change in which the beam was being loaded and the local damage to the flanges. Thus, at this 81 kip load level the delamination failure mode was not observed and instead superseded by an abnormal local flange failure due the manner in which the top of the flange was loaded by the bearing pad (i.e. lateral flange bending).

The predicted total stiffness reduction at the 30 kip load level does not exceed 0.5%. The experimentally observed stiffness reduction for this load level compares well with that predicted, as shown in Figure 21. The data shows noise due to the inherent limitations of the measurements, but the variation in stiffness is no larger than 0.2% at the 30 kip load level. Thus, the results indicate that the off-axis ply damage has little effect on the beam's performance.
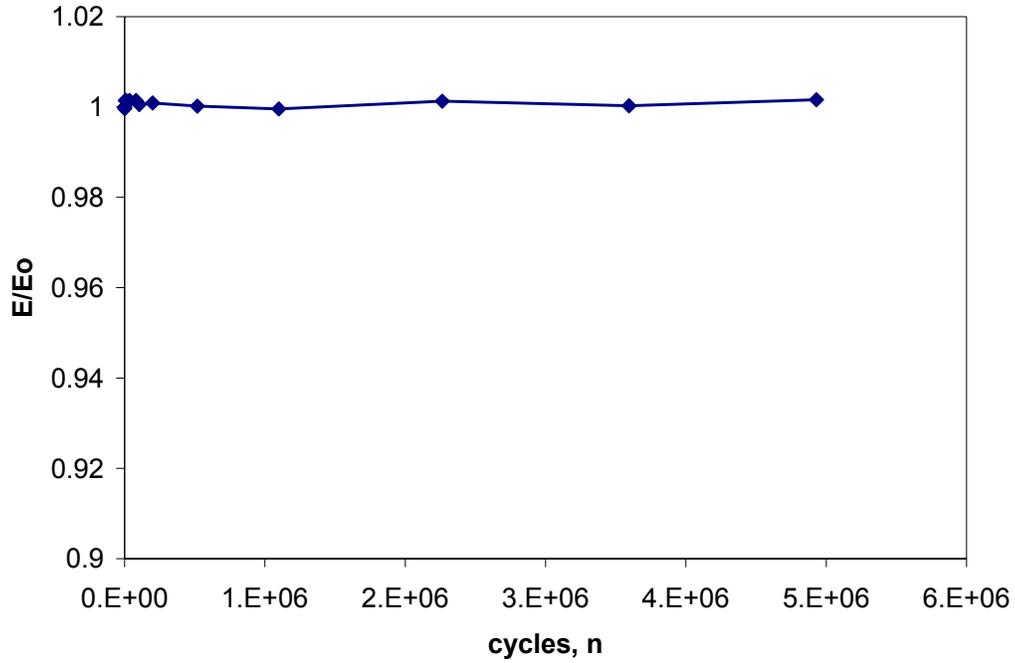
Figure 20. Normalized stiffness reduction for the experimental fatigue test at 30% ultimate capacity.
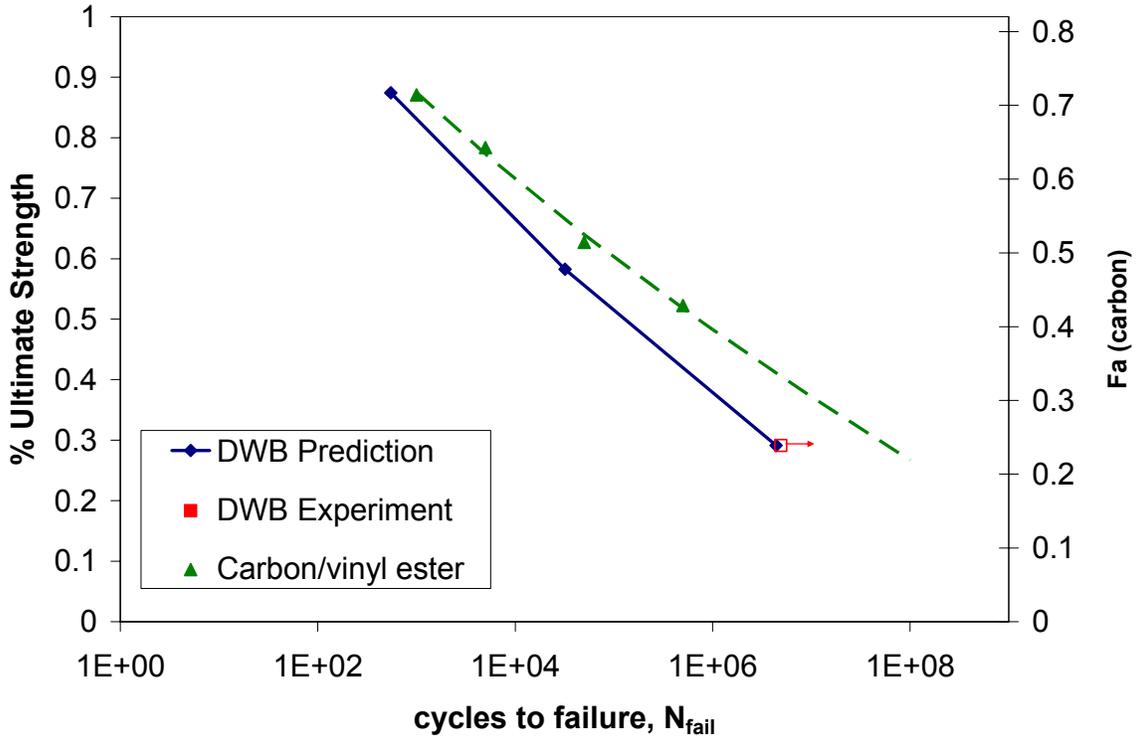

Figure 21. Predicted fatigue life S-N curve for the 11.9 m (39 ft) four-point loading geometry, compared with the experimental data and the carbon fiber fatigue life curve from Verghese (1999)

The result is that the stress level in the critical element, the carbon plies, essentially remains constant over the entire life of the beam. The fact that the ply stress remains constant in the critical element makes the life prediction trivial, as the cycles at failure can be estimated by simply determining the ply stress from the stress analysis and picking off the cycles at failure from the *S-N* curve for the carbon/vinyl ester ply (see Figure 20 and the carbon ply *S-N* curve from Verghese (1999)). It is important, however, to consider the effect of the stress concentration on the fatigue life. A 30 to 45% increase in the carbon ply stress at the load patch may decrease the fatigue life by one or two decades on a logarithmic scale. Therefore, analytical beam models which cannot capture this effect will causes large errors in the predicted fatigue performance.

Given this analysis and testing as compared to the design moment of 224 kip ft is roughly 16% of the capacity (1420 kip-ft). We observed that the DWB can go to 5 million cycles without failure and negligible loss in stiffness at roughly at 26% of the ultimate capacity. Given the average daily traffic of 700 vehicles and assuming that 10% are heavily loaded (close to the design moment), the life of the bridge excluding other degratory affects would be nearly 200 years. Clearly fatigue will not be a failure during the life of the bridge.

CONCLUSIONS AND RECOMMENDATIONS

Based on the live load testing of the Rt. 601 Bridge the following conclusions and recommendations are made:

1. The maximum girder distribution factors for the Rt. 601 Bridge were S/6.0 for interior girders and S/5.1 for exterior girders. These girder distribution factors are less than the girder distribution factors used for the design of the Rt. 601 Bridge. The use of the girder distribution factors in the AASHTO Standard Specification (which are S/4 for interior girders and the lever rule for exterior girders) and AASHTO LFRD Specification for glue-laminated timber decks on steel stringers (which are S/4.5 for interior girders and the lever rule for exterior girders) are recommended for use with glue-laminated timber-FRP girder bridges.

2. The maximum measured dynamic load allowance for the Rt. 601 bridge was 36 %. Slightly larger than the dynamic load allowance used for the design of the Rt. 601 bridge (30 %). In previous research (Neely 2000) a dynamic load allowance of 90 % was measured for a similar bridge with a shorter span and shallower girders. Both of these values are larger than the dynamic load allowances specified in the AASHTO Standard Specification and AASHTO LRFD. It is recommended that further live load testing be conducted of glue-laminated timber deck-FRP girder bridges to further investigate the appropriate value of dynamic load allowance to use for these types of bridges. In the interim it is recommended to use a dynamic load allowance of 50% for glue-laminated timber deck-FRP girder bridges containing the 36 in double web beam.

3. The maximum measured deflection (L/996) of the Rt. 601 Bridge was significantly less than the design deflection of L/800. This can be attributed to bridge stiffening not included in the design of the Rt. 601 bridge. Sources of the additional bridge stiffness are unintended composite action between the girders and timber deck, restraint of girders at the bearings, and differences in the design truck and the test truck.

4. Diaphragms were removed from between girders five through eight to investigate the need of intermediate diaphragms. Small changes were observed in the deflection and structural performance of the bridge. Girder distribution factors were increased a maximum of 12.3 % for interior girders and 7.8 % for exterior girders indicating that using the AASHTO specification girder distribution factors is still conservative. Additionally this indicates that the intermediate diaphragms are not necessary when the AASHTO girder distribution factors are used for bridge design. It is recommended that intermediate diaphragms not be used on glue-laminated timber deck-FRP girder bridges unless they are needed for bracing the girders during construction.

5. Periodic inspections of the Rt. 601 Bridge have found deterioration or damage to the beams. The deterioration/damage was first noted during the Fall 2003 inspection and did not appear to have significantly worsened as of the inspection done during the Summer of 2004. The types of deterioration/damage can be placed in three categories: splinters, blisters, or cracks. The deterioration/damage found is deemed minor with no significant effect on the stiffness or strength of the bridge. Also, the deterioration/damage does not appear to be worsening. It is recommended that VDOT personnel continue performing routine bridge inspections of the Rt. 601 Bridge with any significant change in the condition of the beams (especially lengthening or worsening of the areas in question) communicated to VTRC.

6. A strength based approach to predict delamination onset was followed in which average interlaminar stresses at the critical locations were compared to the interlaminar strengths using the Quadratic Strength Criterion. Detailed finite element analysis of the free edge, utilizing successive sub-models, did not indicate failure at that location. On the other hand, the predicted beam strengths assuming compression failure in the carbon plies of the top flange demonstrated excellent agreement with the experimental data. Therefore, despite the appearance of a delamination failure, the analyses suggest that the actual failure mode is compression. In addition, this analysis was able to capture the span dependence of the moment capacity which was observed experimentally. This span dependence is caused by the stress concentration at the load patch.

7. Based on the assumption of compression failure, a fatigue life prediction was conducted using a remaining strength damage model. Stiffness reductions in the off-axis plies of the tensile flange and sub-flange were modeled using data extrapolated from coupon tests, but the resulting change in the stress level of the critical element was negligible. Therefore, the life at a given applied load level can be predicted simply by determining the stress level in the carbon plies and determining the corresponding cycles to failure

from the fatigue curve for the carbon/vinyl ester material. The validity of the prediction has not yet been verified due to limited fatigue test data.

8. Given this analysis and testing as compared to the design moment of 303 KN-m (224 kip ft) fatigue alone will not produce a failure during the life of the bridge. The estimate life of the bridge would be nearly 200 years, given an average daily traffic count of 700, assuming 10% of the vehicles produce the design moment.

COST AND BENEFITS ASSESSMENT

The Route 601 Bridge in Sugar Grove, VA, spans 39 ft over Dickey Creek. The Bridge is the first to use the Strongwell 36 in deep fiber reinforced polymer (FRP) double web beam (DWB) in a vehicular bridge superstructure. The findings of this report show that the Strongwell 36 in deep FRP beam is a lightweight, durable alternative to conventional structural steel and reinforced concrete beams that can be designed using AASHTO specifications for bridge design. One disadvantage regarding the use of this beam is its cost. The cost per foot of the Strongwell DWB is significantly greater than steel and reinforced concrete beams of similar strength and stiffness. The best uses of the Strongwell beam are ones where the weight savings and/or the improved durability properties will offset the higher initial material costs.

REFERENCES

American Association of State Highway and Transportation Officials (AASHTO) (1996). Standard Specifications for Highway Bridges: Sixteenth Edition. Washington, D.C.

American Association of State Highway and Transportation Officials (AASHTO) (1998). LRFD Bridge Design Specifications: Second Edition. Washington, D.C.

American Association of State Highway and Transportation Officials (AASHTO) (2001). *AASHTO Journal Weekly Transportation Report.* Vol.101, No.8, Feb. 23, 2001.

Bakis, C.E., Bank, L.C., Brown, V.L., Cosenza, E., Davalos, A.M., Lesko, J.J., Machida, A., Rizkalla, S.H., Triantafillou, T.C. (2002). Fiber-Reinforced Polymer Composites for Construction – State-of-the-Art Review. *Journal of Composites for Construction*, Vol.6, No. 2, pp. 73-87.

Barr, P.J., Eberhand, M.O., Stanton, J.F. (2001). Live-Load Distribution Factors in Prestressed Concrete Girder Bridges. *Journal of Bridge Engineering*, Vol. 6, No. 5, pp. 298-305.

Hayes, M. D. (1998). *Characterization of Modeling of a Fiber-Reinforced Polymeric Composite Structural Beam Bridge Structure for Use in the Tom's Creek Rehabilitation Project.* Master's Thesis, Virginia Polytechnic Institute and State University, Blacksburg, VA.

Hyer, M.D. (1998). *Stress Analysis of Fiber-Reinforced Composite Materials*, WCB/McGraw Hill, New York.

M. D. Hayes, J.J. Lesko, J. Haramis, T. E. Cousins, J. Gomez, P. Massarelli, Laboratory & Field Characterization of the Tom's Creek Bridge Composite Superstructure. *Journal of Composites for Construction*, Vol. 4, No. 3, August 2000, pp. 1-9.

Hayes, M.D. Lesko, J.J., Cousins, T.E., Waldron,C., Witcher, D. Barefoot,G. & Gomez, J., (2001) "Design of a Short Span Bridge Using FRP Girders," Composites in Construction International Conference, October 10-12, 2001, Porto, Portugal.

Kassner, B. L. (2004). *Long-Term In-Service Evaluation of Two Bridges Designed with Fiber-Reinforced Polymer Girders*. Master's Thesis, Virginia Polytechnic Institute and State University, Blacksburg, VA.

Kliger, H.S. and Loud, S. (2001). "Composites Growth in the Infrastructure Market," *46th International SAMPE Symposium*, May 6-10, 2001. pp. 952-955.

Neely, W. D. Jr. (2000). *Evaluation of In-Service Performance of the Tom's Creek Bridge*. Master's Thesis, Virginia Polytechnic Institute and State University, Blacksburg, VA.

Nystrom, H., Watkins, S.E., Nanni, A., and Murray, S. Financial Viability of Fiber-Reinforced Polymer (FRP) Bridges. *Journal of Management Engineering,* pending publication.

Paultre, Patrick, Chaallal, Omar, and Proulx, Jean (1991). Bridge dynamics and dynamic amplification factors – a review of analytical and experimental findings, *Canadian Journal of Civil Engineering*, Vol. 19, pp. 260-278.

Reifsnider, K.L., and Case, S. W., (2002), *Damage Tolerance & Durability of Material Systems*. Wiley,

Restrepo, E.S. (2002). *Determination of AASHTO Bridge Design Parameters through Field Evaluation of the Rt. 601 Bridge: A Bridge Utilizing Strongwell 36 in. Fiber-Reinforced Polymer Double Web Beams as the Main Load Carrying Members*. Master's Thesis, Virginia Polytechnic Institute and State University, Blacksburg, VA.

J. Senne, J. J. Lesko, & S. Case, (2000) A Life Prediction Methodology for Thick Section Composites Used in Civil Infrastructure. *ASTM Journal of Composite Science & Technology*, Vol. 22, No. 4, pp. 241-248.

Stallings, J.M. and Yoo, C.H. (1993). Tests and Ratings of Short-Span Steel Bridges. *Journal of Structural Engineering*, Vol. 119, No. 7, pp. 2150-2167.

Stallings, J.M., Cousins, T.E., Tedesco, J.W. (1996). *Fatigue of Diaphragm-Girder Connection. Executive Summary RP 930-307,* Auburn University, April 1996.

Strongwell. 2000. EXTREN^{TM} Design Guide.

Structural Testing Incorporated (STI).(1998). Field Test of Washington Schoolhouse Lane
Bridge. *Report to HardCore Composites*, Dec. 7, 1998.

Verghese, K.E., (1999), *Durability of Polymer Matrix Composites for Infrastructure: The Role of
the Interphase*. Master's Thesis, Virginia Polytechnic Institute and State University:
Blacksburg, VA.

Virginia Department of Motor Vehicles (DMV) (2000). Motor Carrier Service Operations.
Richmond, VA.

Waldron, C.J. (2001). Determination of the Design Parameters for the Route 601 Bridge: A
Bridge Containing the Strongwell 36 in. Hybrid Composite Double Web Beam. Master's
Thesis, Virginia Polytechnic Institute and State University, Blacksburg, VA.